Available online at www.sciencedirect.com
ScienceDirect
Physica D 234 (2007) 105–123
PHYSICA D
www.elsevier.com/locate/physd

Parametric smoothness and self-scaling of the statistical properties of a minimal climate model: What beyond the mean field theories?

Valerio Lucarini[a,b,*], Antonio Speranza[a], Renato Vitolo[a]

[a] *PASEF – Physics and Applied Statistics of Earth Fluids, Dipartimento di Matematica ed Informatica, Università di Camerino, Camerino (MC), Italy*
[b] *Department of Physics, University of Bologna, Bologna, Italy*

Received 9 October 2006; received in revised form 2 July 2007; accepted 8 July 2007
Available online 14 July 2007

Communicated by U. Frisch

Abstract

A quasi-geostrophic intermediate complexity model of the mid-latitude atmospheric circulation is considered, featuring simplified baroclinic conversion and barotropic convergence processes. The model undergoes baroclinic forcing towards a given latitudinal temperature profile controlled by the forced equator-to-pole temperature difference T_E. As T_E increases, a transition takes place from a stationary regime – Hadley equilibrium – to a periodic regime, and eventually to a chaotic regime where evolution takes place on a strange attractor. The attractor dimension, metric entropy, and bounding box volume in phase space have a smooth dependence on T_E, which results in power-law scaling properties. Power-law scalings with respect to T_E are detected also for the statistical properties of global physical observables — the total energy of the system and the averaged zonal wind. The scaling laws, which constitute the main novel result of the present work, can be thought to result from the presence of a statistical process of baroclinic adjustment, which tends to decrease the equator-to-pole temperature difference and determines the properties of the attractor of the system. The self-similarity could be of great help in setting up a theory for the overall statistical properties of the general circulation of the atmosphere and in guiding – on a heuristic basis – both data analysis and realistic simulations, going beyond the unsatisfactory mean field theories and *brute force* approaches. A leading example for this would be the possibility of estimating the sensitivity of the output of the system with respect to changes in the parameters.

Keywords: Atmospheric circulation; Climate model; Chaotic dynamics; Strange attractor; Attractor dimension; Metric entropy; Bonding box; Scaling law; Self-similarity

1. Introduction

The understanding of climate is a scientific issue as well as being also of practical importance, since it is connected to aspects of vital importance for human life and environment. Recently, climate has also become a politically relevant issue. In this paper we propose our scientific approach and some encouraging results concerning the theory of General Atmospheric Circulation (GAC) – the core machine of weather and climate – looked upon as a problem in physics. We note here that there may be evidence that our understanding of the dynamical processes determining climate, and its evolution, is somewhat lagging behind our ability in setting up (often somewhat gigantic) simulation models of the climatic system [53] and, as a consequence, from the proposed effort great benefits can come to our ability to diagnose and/or construct climate models.

1.1. The climatic system

Climate is defined as the set of the statistical properties of the climatic system. In its most complete definition, the climatic system is composed of four intimately interconnected sub-systems, atmosphere, hydrosphere, cryosphere, and biosphere.

* Corresponding address: Department of Mathematics and Computer Science, University of Camerino, Via Madonna delle Carceri, 62032 Camerino, MC, Italy. Tel.: +39 3476141563.
E-mail addresses: lucarini@alum.mit.edu, lucarini@adgb.df.unibo.it (V. Lucarini).

0167-2789/$ - see front matter © 2007 Elsevier B.V. All rights reserved.
doi:10.1016/j.physd.2007.07.006

These subsystems interact nonlinearly with each other on various time–space scales [51,59]. The atmosphere is the most rapid component of the climatic system, is very rich in microphysical structure and composition, and evolves under the action of macroscopic driving and modulating agents — solar heating and Earth's rotation and gravitation, respectively. The atmospheric circulation is the basic engine which transforms solar heating into the energy of the atmospheric motions and determines the bulk of weather and climate as we commonly perceive them. The atmosphere features both many degrees of freedom, making it complicated, and nonlinear interactions of several different components involving a vast range of time scales, which makes it complex. The dynamics of such a system is chaotic and is characterized by a very wide spectrum of natural (*i.e.* internally generated) variability [48]. The understanding of the physical mechanisms operating in the atmosphere critically influences important human activities like weather forecasting, territorial planning, etc. This is one of the reasons why von Neumann positioned atmospheric dynamics in the core of the ongoing development of numerical modeling [14]. The GAC also poses problems of a general physical nature as a realization of planetary scale thermodynamic transformations in a rotating, stratified fluid. Among all the physical processes involved in the GAC, the baroclinic conversion plays a central role because it is through this mechanism that rotating, stratified fluids convert the available potential energy [45], stored in the form of thermal fluctuations, into the vorticity and kinetic energy of the air flows. At mid-latitudes of both hemispheres, the baroclinic conversion process can be taken as the main process responsible for the destabilization of any hypothetical stationary circulation (fixed point, in the terminology of dynamical systems theory) of the atmosphere, in particular that given by the zonally (longitudinally) symmetric atmospheric circulation characterized by a purely zonal (west to east) wind (jet) [36]. Note that these theoretically computed stationary circulations correspond to values of the field variables way out of the observed range: the zonal solution is characterized by winds of the order of 100 ms^{-1} and the latitudinal (equator–pole) temperature difference to the order of 100 K. Both of these values are about twice as large as what actually observed. Apart from the classical role of baroclinic instability [12,19] in mid-latitude weather development [21,22,76], different forms of baroclinic conversion can be actually observed, both at larger scales (*e.g.* in the ultralong planetary waves associated with the so called low frequency variability [5,6,15,68]) and at smaller scales (*e.g.* in the banded sub-frontal structures [55]). The definition of the basic ingredients in the physical mechanism of baroclinic conversion is to be considered one the main successes of the dynamical meteorology of the past century.

1.2. Classical theories of GAC and associated problems

Historically – see the classical monograph by Lorenz [47] – the problem of GAC has been essentially approached in terms of analyzing the time-mean circulation. Usual separations such as between time average and fluctuations or between the zonal and the eddy field, are somewhat arbitrary, but perfectly justifiable with arguments of symmetry, evaluation of statistical moments, etc. The time average–fluctuations separation is often suggestive of a theory in which the fluctuations growing on an unstable basic state, identified in the time average, feed back onto the basic state itself and *stabilize* it. The central objective of the classical circulation theory is the *closure* in the form of a *parameterization* of the nonlinear eddy fluxes in terms of quantities which can be derived from the mean field itself. Extremely important and interesting theories of this kind – *e.g.* baroclinic instability – have been formulated throughout the whole history of meteorology and have substantially improved our understanding of the basic dynamical processes underlying the observed evolution of the atmospheric system. However, in general this approach is not only unsuccessful, it is just not feasible. The basic reason is that the stability properties of the time-mean state do not provide even a zeroth-order approximation of the dynamical properties of the full nonlinear system. This has been illustrated by theoretical arguments [24] and simple counter-examples of physical significance (see *e.g.*, [54,78]). As a consequence, it is not possible to create a self-consistent theory of the time-mean circulation relying only on the time-mean fields, since a parameterization of eddy fluxes in terms of quantities derivable from the mean field is useless: the average state does not carry the necessary physical information.

Alternative approaches have been proposed, *e.g.* mimicking the GAC via dynamical systems approach with simplified low dimensional models, say below 10 degrees of freedom (see *e.g.* [34]). However, the physical relevance and mathematical generality of these approaches has been criticized as well, whereas the relevance of the space–time geophysical scaling behavior has been emphasized [69]. Nevertheless, a comprehensive and coherent picture of the GAC is still far from being available and the classical *time-mean* approach has not been completely abandoned as a paradigm.

1.3. Some consequences of the failure of classical GAC theories

It is clear that in the context of the classic paradigm of GAC, the main task of modeling consists in capturing the mean field: the fluctuations will follow as its instabilities. This point of view, whether explicit or not, has strongly influenced the set-up and diagnostics of existing General Circulation Models (GCMs). As a consequence, the diagnostic studies usually focus on comparing the temporal averages of the simulated fields rather than on analyzing the representation of the dynamical processes provided by the models. Similar issues are related to the provision of the so-called extended range weather forecasts. Suppose, in fact, that the forecaster was given the next month average atmospheric fields: what practical information could he/she derive from that? Of course, if dynamical information were stored in the average fields – typically in the form of dominant regimes of instability derivable from the time-mean flow – he/she could obtain useful information from the prediction of such time-mean fields. Unfortunately, as remarked

above, such a picture has proved to be far from being applicable, and the problem of extended range forecast is still open even in terms of clearly formulating what we should forecast in place of average fields.

1.4. The statistical mechanical point of view

Conspicuous difficulties were encountered [3,44] while trying to construct a Climate Change theory on the basis of fluctuation–dissipation theorems [42]. The main problem is that the climate system may be considered as a forced and dissipative chaotic system, featuring properties such as the non-equivalence between the external and internal fluctuations [49]. The reason for this non-equivalence is that, by dissipation, the attractor of the system lives on a manifold of zero volume inside phase space [20] (although a small amount of noise, which is always present in physical systems, smooths the invariant measure corresponding to the attractor [65]): the internal natural fluctuations occur within such a manifold whereas externally induced fluctuations move the system out of the attractor with probability one. In this sense, generalizations of the fluctuation–dissipation theorem have been recently established for certain systems having a chaotic attractor. Ruelle [67] has proved a generalization of the fluctuation–dissipation theorem for Axiom-A attractors (such systems carry a unique, zero-noise SRB measure [81]). Furthermore, some specific examples have been provided in [11] and a further extension to finite perturbations has been recently obtained [8]. At numerical level, Kramers–Kronig relations [52] have been recently verified [62] also for the linear response of the Lorenz-63 system [46], which is non-hyperbolic. Nevertheless, to the best knowledge of the authors, rigorous applications of these results to the case of GAC have never been performed.

A naturally ensuing scientific goal is to derive simplified equations of motion (*minimal models*). The project of writing the equations describing the statistics of the system *directly on the attractor* (by projection) has been carried on with great attention in the recent past, but, despite the big efforts, no applicable result has been obtained so far and basic difficulties have emerged [28,31,50].

1.5. The brute force approach

The public attention on Climate Change issues has motivated in recent years an enormous increase in the number of degrees of freedom (up to 10^6 and beyond) of the most recent Global Circulation Models (GCMs) and in the complexity of the physical processes included in them [39]. In the absence of robust and efficient scientific paradigms, a gap was created between the studies revolving around phenomenological and/or numerical modeling issues and those focused on fundamental mechanisms of GAC [35]. Note that the assumption that adopting models of ever increasing resolution (allowed by the larger and larger availability of computer power) will eventually lead to the final understanding of the GAC (a sort of *brute force* approach) is not based on any consolidated mathematical knowledge and may, in fact, be misleading. One basic reason is that, in the limit of infinite resolution for any numerical model of fluid flow, the convergence to the statistical properties of the continuum real fluid flow dynamics is not guaranteed. At the present stage, most of the leading climate models are neither consistent nor realistic even in the representation of the basic time–space spectral properties of the variability of the atmosphere at mid-latitudes [53].

1.6. Numerical modeling, smoothness and limited variability

In the modeling activity we have to deal with three different kinds of attractors: the attractor of the real atmosphere; the reconstruction of the real attractor from observations; the attractors of the model (maybe more than one) we adopt in climatic studies. As for the second one, the (presumably) best reconstructions available are provided by the reanalyses. Reanalyses are obtained by means of variational adaptation (in simple quadratic error model–observations measure) of a climate model trajectory to observations. Note that many of the operations that are practically performed when executing reanalysis (*e.g.*, local linearizations in phase space) require properties of local smoothness in phase space. Presently there are two alternative main global reanalyses, which feature distinct statistical properties, albeit obviously in broad agreement. Details can be found, *e.g.*, in [21,22,68]. As for the third kind of attractors, the various GCMs almost surely possess substantially different attractors, which reflects disagreements in the statistical properties of the atmosphere [53]. In the fundamental effort of bringing a model into statistical agreement with the reanalyses (taken as best guess of the real atmosphere), a key role is played by the smoothness and the limited variability of the statistical properties of the model as a function of the tunable parameters. Note that if the statistical properties of a model feature a too strong dependence on the tunable parameters, the *shooting* to the target of the statistical properties of reanalyses would be prohibitively difficult and ill-defined.

Actually, the properties of low dimensional prototypes of atmospheric circulation are rather discouraging in this respect (see e.g. [9]), since small changes in the values of the model parameters may cause dramatic variations of the resulting climate. However, a sort of common wisdom among modelers has always been that with the increase in the number of degrees of freedom the statistical properties could somewhat regularize the discontinuous dependence on external parameters that characterizes many small dimensionality models. See e.g. [1,2].

1.7. Our approach

Our approach focuses on the following question: once we abandon the unsatisfactory mean field theories, what may come next? More specifically, what can we do for developing a new approach to a theory of GAC which can serve as a guidance for setting up and diagnosing GCMs? Which statistical properties may be crucial? In so doing, we are, at this stage, not seeking realism in the model representation of

atmospheric dynamics, but rather searching for representations of key nonlinear processes with the minimum of ingredients necessary to identify the properties under investigation. We have decided to choose a rather simplified quasi-geostrophic (QG) model with just a few hundreds degrees of freedom, able to capture the central process of the GAC, *i.e.* the ordinary baroclinic conversion in the mid-latitude atmospheric jet. Other atmospheric processes, acting on longer or shorter spatial and temporal scales, such as those mentioned before, are essentially excluded. The model is vertically discretized into two layers, which is the minimum for baroclinic conversion to take place [58,60], and latitudinally discretized by a Fourier half-sine pseudospectral expansion up to order JT. We have used $JT = 8, 16, 32, 64$, yielding a hierarchy of QG models having increasing phase space dimension. A fundamental property of these models is almost-linearity: the eddy field is truncated to one wavenumber in the longitudinal (zonal) direction, which entails the evolution equation of the waves to be linear in terms of the time-varying zonal flow. This provides a dynamical meaning for the separation between zonal and eddy flow, where the zonal wind acts effectively as an integrator. The model considered here has extensively been used in nonlinear modeling analysis since the '80s [54,78] and, more recently, has been adopted as a dynamical simulator for analysis of extremes [26,27]. Of course, today there is a vast choice of readily available analogous or more *realistic* models, which can be run with ease with easily available computer facilities, but our choice of *intermediacy* between very low dimensional models and GCMs allows for a detailed check of all the statistical properties of the model dynamics.

1.8. The structure of the paper

In Section 2 we present a brief derivation of the evolution equations for the two-layer QG model. This derivation allows a clear understanding of the physics involved in the considered hierarchy of QG equations. The main results of this work are presented in Sections 3 and 4. We study the sensitivity of the model behavior with respect to the parameter T_E determining the forced equator-to-pole temperature gradient, which acts as baroclinic forcing. The influence of the order of (spectral) discretization in the latitudinal direction is also analyzed. In Section 3 we characterize the transition from stationary to chaotic dynamics and study the dependence on T_E and on model resolution JT of the dimension of the strange attractor, of the metric entropy, and of the volume of its bounding box in the phase space. In Section 4 we analyze the statistical properties of two physically meaningful observables (functions of state space variables), namely the total energy of the system and the latitudinally averaged zonal wind. An inspection of the latitudinal wind profiles is also presented. In Section 5 a discussion is given of the properties observed for the present model in terms of dynamical systems theory and of the relevant physical implications. In Section 6 we give our conclusive remarks and perspectives for future works. In the Appendix we present the set of differential equations examined in this study and sketch the numerical methods adopted.

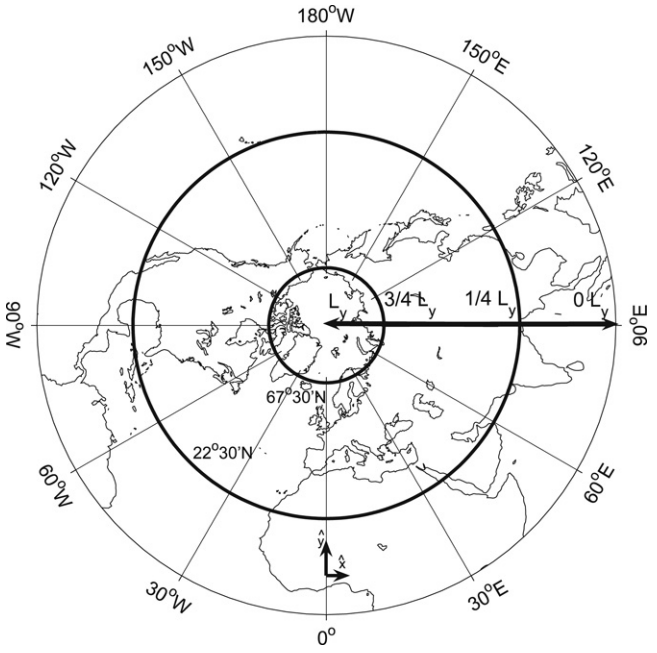

Fig. 1. Sketch of the actual geographical area corresponding to the simplified β channel. The local x and y directions and the β-channel width L_y are indicated. The mid-latitudes range from $1/4L_y$ to $3/4L_y$, corresponding to a 45° latitudinal belt centered at 45° N.

2. The model

The description of the large scale behavior of the atmosphere is usually based on the systematic use of dominant balances, which are derived on a phenomenological diagnostic basis, but whose full correctness at theoretical level is still unclear. When considering the dynamics of the atmosphere at mid-latitudes, on spatial and temporal scales comparable with or larger than those of the synoptic weather (about 1000 km and 1 day, respectively), the hydrostatic and geostrophic balances are phenomenologically well established. From the set of *ab-initio* dynamic and thermodynamic equations of the atmosphere it is possible to obtain a set of simplified prognostic equations for the synoptic weather atmospheric fields in a domain centered at mid-latitudes – the QG equations – by assuming that the fluid obeys the hydrostatic balance and undergoes small departures from the geostrophic balance [13,58,77]. A great number of physical phenomena are *filtered out* of the equations by the QG approximation: various types of waves associated with strong local divergence, turbulent motions, etc. Again, there is no doubt that these are small on the time–space scales of the motions we consider. However, it is still an open question to what extent they influence or not the statistics of large scale atmospheric motions and, in case, how to model such a statistical effect. Note also that in general the QG attractor is not a good approximation to the attractor of the corresponding full *ab-initio* equations, despite the fact that the QG balance approximation is diagnostically quite good for the dominating time–space scales of the atmosphere [50].

In this work we consider a β-*channel* periodic domain, with $\in \mathbf{R}/2\pi L_x$ denoting the zonal and $y \in [0, L_y]$ the latitudinal coordinate (see Fig. 1). As a further approximation,

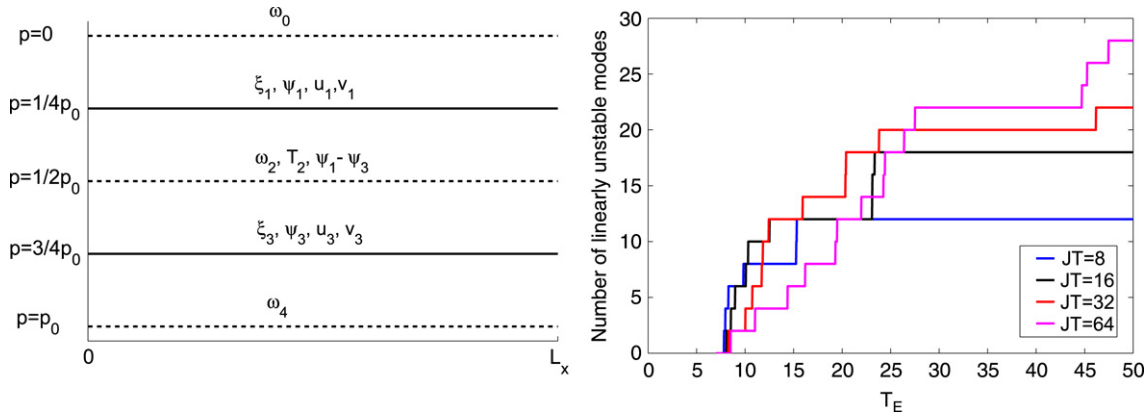

Fig. 2. Left: Sketch of the vertical–longitudinal section of the system domain. The domain is periodic in the zonal direction x with wavelength L_x. At each pressure level, the relevant variables are indicated. Right: Number of linearly unstable modes at the Hadley equilibrium as a function of the parameter T_E for $JT = 8, 16, 32, 64$.

we consider only two vertical layers [60]. This is the minimal system retaining the baroclinic conversion process, which is the basic physical feature of the QG approximation. We refer to the left panel of Fig. 2 for a sketch of the vertical geometry of the two-layer system. In order to avoid problems in the definition of the boundary conditions of the model, due to the prescription of the interaction with the polar and the equatorial circulations at the northern and southern boundary, respectively, we consider a domain extending from the pole to the equator. Of course, near the equator the QG approximation is not valid, so that the representation of the actual tropical circulation is beyond the scope. The equations of motions are:

$$D_t^1 \left(\Delta_H \psi_1 + f_0 + \beta y\right) - f_0 \frac{\omega_2 - \omega_0}{\delta p} = 0, \tag{1}$$

$$D_t^3 \left(\Delta_H \psi_3 + f_0 + \beta y\right) - f_0 \frac{\omega_4 - \omega_2}{\delta p} = 0, \tag{2}$$

$$D_t^2 \left(\frac{\psi_1 - \psi_3}{\delta p}\right) - H_2^2 \frac{f_0}{p_2^2} \omega_2 = \kappa \Delta_H \left(\frac{\psi_1 - \psi_3}{\delta p}\right) + \frac{R}{p_2 f_0} \frac{Q_2}{C_p} \tag{3}$$

where f_0 is the Coriolis parameter and β its meridional derivative evaluated at the center of the channel, κ parameterizes the heat diffusion, R and C_p are the thermodynamical constants for dry air, Δ_H is the horizontal laplacian operator. Moreover, the streamfunction ψ_j is defined at pressure levels $p = p_{j=1} = p_0/4$ and $p = p_{j=3} = 3/4 p_0$, while the vertical velocity ω is defined at the pressure levels $p = p_{j=0} = 0$ (top boundary), $p = p_{j=2} = p_0/2$, and $p = p_{j=4} = p_0$ (surface boundary). The pressure level pertaining to the discrete approximation to vertical derivative of the streamfunction $\partial \psi_g / \partial p$ as well as the stratification height H is $p = p_{j=2}$, and $\delta p = p_3 - p_1 = p_2 = p_0/2$. Q_2 is the diabatic heating, and D_t^j is the usual Lagrangian derivative defined at the pressure level p_j, $D_t^j \bullet = \partial_t + J\left(\psi_j, \bullet\right)$, where J is the conventional Jacobian operator defined as $J(A, B) = \partial_x A \partial_y B - \partial_y A \partial_x B$. The streamfunction at the intermediate level p_2 is computed as average between the streamfunctions of the levels p_1 and p_3, so that the material derivative at the level p_2 can be expressed as $D_t^2 = 1/2(D_t^1 + D_t^3)$.

We choose the following simple functional form for the diabatic heating:

$$Q_2 = \nu_N C_p \left(T^\star - T\right) = \nu_N C_p \frac{f_0 p_2}{R} \left(\frac{2\tau^\star}{\delta p} - \frac{\psi_1 - \psi_3}{\delta p}\right), \tag{4}$$

where the temperature T is evaluated at the pressure level 2 and is defined via hydrostatic relation, which implies that the system is relaxed towards a prescribed temperature profile $T^\star$ with a characteristic time scale of $1/\nu_N$. $T^\star$ and $\tau^\star$ are respectively defined as follows:

$$T^\star = \frac{T_E}{2} \cos\left(\frac{\pi y}{L_y}\right), \qquad \tau^\star = \frac{R}{f_0} \frac{T_E}{4} \cos\left(\frac{\pi y}{L_y}\right), \tag{5}$$

so that T_E is the forced temperature difference between the low and the high latitude border of the domain. In our simulations we assume no time dependence for the forcing parameter T_E, thus discarding the seasonal effects. Since by thermal wind relation $\left(\vec{u}_1 - \vec{u}_3\right)/\delta p = \hat{k} \times \vec{\nabla} / \left(\psi_1 - \psi_3\right)/\delta p$, we have that the diabatic forcing Q_2 in (4) causes a relaxation of the vertical gradient of the zonal wind $u_1 - u_3$ towards the prescribed profile $2m^\star = 2\mathrm{d}\tau^\star/\mathrm{d}y$, where the constant 2 has been introduced for later convenience.

By imposing $\omega_0 = 0$ (top of the atmosphere) and assuming $\omega_4 = -E_0 \Delta_H \psi_3$ (Ekman pumping [58]), and after a rearrangement of Eqs. (1)–(3), one obtains the evolution equations for the baroclinic field $\tau = 1/2\left(\psi_1 - \psi_3\right)$ and the barotropic field $\phi = 1/2\left(\psi_1 + \psi_3\right)$:

$$\partial_t \Delta_H \tau - \frac{2}{H_2^2} \partial_t \tau + J\left(\tau, \Delta_H \phi + \beta y + \frac{2}{H_2^2} \phi\right) + J\left(\phi, \Delta_H \tau\right) = \frac{2\nu_E}{H_2^2} \Delta_H \left(\phi - \tau\right) - \frac{2\kappa}{H_2^2} \Delta_H \tau + \frac{2\nu_N}{H_2^2} \left(\tau - \tau^\star\right), \tag{6}$$

$$\partial_t \Delta_H \phi + J\left(\phi, \Delta_H \phi + \beta y\right) + J\left(\tau, \Delta_H \tau\right) = -\frac{2\nu_E}{H_2^2} \Delta_H \left(\phi - \tau\right) \tag{7}$$

Table 1
Variables of the system and non-dimensionalization factors

Variable	Scaling factor	Value of scaling factor
x	l	10^6 m
y	l	10^6 m
t	$u^{-1}l$	10^5 s
ψ_1	ul	10^7 m^2 s^{-1}
ψ_3	ul	10^7 m^2 s^{-1}
ϕ	ul	10^7 m^2 s^{-1}
τ	ul	10^7 m^2 s^{-1}
A_n^1	ul	10^7 m^2 s^{-1}
B_n^1	ul	10^7 m^2 s^{-1}
A_n^2	ul	10^7 m^2 s^{-1}
B_n^2	ul	10^7 m^2 s^{-1}
m	u	10 ms^{-1}
U	u	10 ms^{-1}
m_n	u	10 ms^{-1}
U_n	u	10 ms^{-1}
w_n	l^{-1}	10^{-6} m^{-1}
Lag	$u^{-1}l$	10^5 s
λ_j	ul^{-1}	10^{-5} s^{-1}
t_p	$u^{-1}l$	10^5 s
T	ulf_0R^{-1}	3.5 K
E	$u^2l^2(\delta p)g^{-1}$	5.1×10^{17} J

For A_n^1, B_n^1, A_n^2, B_n^2, m_n, U_n, and w_n, the index n ranges from 1 to JT. For λ_j, $n = 1, \ldots, 6 \times JT$.

where $\nu_E = f_0 E_0 H_2^2/(2\delta)$ is the viscous-like coupling between the free atmosphere and the planetary boundary layer via Ekman pumping, and the meaning of $\tau^\star$ is made clear. Notice that this system features only quadratic nonlinearities.

The two-layer QG system (6) and (7) can be brought to the non-dimensional form, which is more usual in the meteorological literature and is easily implementable in computer codes. This is achieved by introducing length and velocity scales l and u and performing a non-dimensionalization of both the system variables (x, y, t, ϕ, τ, T) (as described in Table 1) and of the system constants (Table 2); in our case appropriate values are $l = 10$ m^6 and $u = 10$ ms^{-1}.

In this work we consider a simplified spectral version of Eqs. (6) and (7), where truncation is performed in the zonal Fourier components so that only the zonally symmetric component and one of the non-symmetric components are retained. The derivation is reported in [54,78]. The main reason for this choice is that we wish to focus on the interaction between the zonal wind and waves, thus neglecting the wave–wave nonlinear interactions. Since quadratic nonlinearities generate terms with Fourier components corresponding to the sum and difference of the Fourier components of the two factors, we can exclude direct wave–wave interactions provided that we only retain a single wave component (see, *e.g.*, [52] for a general discussion of these effects in a different context). Note that if cubic nonlinearities were present, direct self-wave–wave interaction would have been possible [5]. In the present case, the wave can self-interact only indirectly through the changes in the values of the zonally symmetric fields. This amounts to building up equations which are *almost-linear*, in the sense that the wave dynamics is linear with respect to the zonally symmetric parts of the fields (*i.e.*, the winds). The wavelength of the only retained wave component is $L_x/6$, since we intend to represent the baroclinic conversion processes, which in the real atmosphere take place on scales of $L_x/6$ or smaller [21]. In so doing we are retaining only one of the classical ingredients of GAC, i.e. the *zonal wind–wave* interaction.

Both ϕ and τ are thus determined by three real fields: the zonally symmetric parts and the real and imaginary part of the only retained zonal Fourier component. A pseudospectral decomposition with JT modes is then applied to the resulting 6 real fields in the y-direction, yielding a set of $6 \times JT$ ordinary differential equations in the spectral coefficients. For the truncation order JT we have used the values $JT = 8, 16, 32, 64$.

This is the prototypal model we use as *laboratory* for the analysis of the GAC. The only form of realism we are trying to achieve here is that the statistical properties of the nonlinear cycle *baroclinic instability — barotropic & baroclinic stabilization* are represented.

3. Dynamical and statistical characterization of the model attractor

The purpose of this section is to show that the *zonal wind–wave* system captures the nonlinear process of baroclinic conversion and *barotropic–baroclinic* stabilization displaying simple (self-scaling, in fact), smooth, robust global behavior

Table 2
Values of the parameters used in this work and adimensionalization factors

Parameter	Dimensional value	Non-dimensional value	Scaling factor	Value of scaling factor
L_x	2.9×10^7 m	29	l	10^6 m
L_y	10^7 m	10	l	10^6 m
χ	$2\pi/(4.833 \times 10^6)$ m^{-1}	1.3	l^{-1}	10^{-6} m^{-1}
H_2	7.07×10^5 m	7.07×10^{-1}	l	10^6 m
f_0	10^{-4} s^{-1}	10	ul^{-1}	10^{-5} s^{-1}
β	1.6×10^{-11} m^{-1} s^{-1}	1.6	ul^{-2}	10^{-11} m^{-1} s^{-1}
ν_E	5.5×10^5 m^2 s^{-1}	5.5×10^{-2}	ul	10^7 m^2 s^{-1}
κ	2.8×10^5 m^2 s^{-1}	2.8×10^{-2}	ul	10^7 m^2 s^{-1}
ν_N	1.1×10^{-6} s^{-1}	1.1×10^{-1}	ul^{-1}	10^{-5} s^{-1}
T_E	28–385 K	8–110	ulf_0R^{-1}	3.5 K

Our system is equivalent to that of Malguzzi and Speranza [78], where the following correspondences hold $1/(H_2^2) \leftrightarrow F$, $(2\nu_E)/(H_2^2) \leftrightarrow \nu_E/2$, $(2\kappa)/(H_2^2) \to \nu_S$, and $\nu_N \leftrightarrow \nu_H$.

Table 3
Approximate values of the parameter T_E where the Hadley equilibrium loses stability via Hopf bifurcation (T_E^H) and where the onset of the chaotic regime occurs (T_E^{crit}) for each of the considered orders of truncation JT

JT	T_E^H	T_E^{crit}
8	7.83	9.148
16	8.08	8.415
32	8.28	8.522
64	8.51	8.663

See text for details.

for parameter values of physical relevance. In Section 3.1 we briefly sketch the routes to chaos in our model. The scaling laws in the fully chaotic regime are then analyzed by studying the Lyapunov exponents (Section 3.2) and the bounding box (Section 3.3).

3.1. Bifurcations at the transition to chaos

The system of equations (6) and (7) has the following stationary solution for zonally symmetric flows:

$$\phi(y) = \tau(y), \tag{8}$$

$$\frac{2\kappa}{H_2^2}\frac{\mathrm{d}^2\tau(y)}{\mathrm{d}y^2} + \frac{2\nu_N}{H_2^2}\left(\tau(y) - \tau^\star(y)\right) = 0. \tag{9}$$

Considering the functional form (5) for $\tau^\star(y)$, the following temperature profile $T(y)$ is realized:

$$T(y) = \frac{T_E}{2}\frac{\cos\left(\frac{\pi y}{L_y}\right)}{1+\frac{\kappa}{\nu_N}\left(\frac{\pi}{L_y}\right)^2} = \frac{T^\star(y)}{1+\frac{\kappa}{\nu_N}\left(\frac{\pi}{L_y}\right)^2}. \tag{10}$$

This solution describes a zonally symmetric circulation characterized by the stationary balance between the horizontal temperature gradient and the vertical wind shear, which corresponds on the Earth system to the idealized pattern of the Hadley equilibrium [36,58].

There is a value of the equator-to-pole temperature gradient T_E^H such that if $T_E < T_E^H$ the Hadley equilibrium (8) and (9) is stable and has an infinite basin of attraction, whereas if $T_E > T_E^H$ it is unstable. In the stable regime with $T_E < T_E^H$, after the decay of transients, the fields ϕ, τ, and T are time independent and feature zonal symmetry — they only depend on the variable y. Moreover, they are proportional by the same near-to-unity factor to the corresponding relaxation profiles, compare (8)–(10). In particular, this implies that all the equilibrium fields are proportional to the parameter T_E.

When increasing the values of the control parameter T_E beyond T_E^H, the equilibrium described by (8) and (9) becomes unstable: a complex conjugate pair of eigenvalues of the linearization of (A.4)–(A.9) at the equilibrium (8) and (9) cross the imaginary axis and their real part turns positive. This suggests the occurrence of a Hopf bifurcation. The corresponding physical scenario is the following: for high values of the meridional temperature gradient the Hadley equilibrium is unstable with respect to the process of baroclinic conversion, which allows the transfer of available potential energy of the zonal flow stored into the meridional temperature gradient into energy of the eddies [12,19].

A stable periodic orbit branches off from the Hadley equilibrium (8) and (9) as T_E increases above T_E^H. The attracting periodic orbit persists for a narrow interval of T_E, and for slightly larger values of T_E, *i.e.* $T_E > T_E^{\mathrm{crit}}$, a strange attractor appears. Describing in detail the route to the formation of the strange attractor is beyond the scope of the present paper: this problem will be tackled elsewhere. Suffice here to say that, in the case of $JT = 16$, 32 and 64, this route involves the breakdown of a two-torus attractor of the flow and is very similar to those described in [9,61]. The observed values of T_E^H and T_E^{crit} typically increase with the considered truncation order JT. Results are reported in Table 3 for the choice of constants reported in Table 2. A finer resolution allows for more efficient stabilizing mechanisms, which counteract the baroclinic instability, because they act preferentially on the small scales. Such mechanisms are the barotropic stabilization of the jet, increasing the horizontal shear through the convergence of zonal momentum, which is proportional to the quadrature of the spatial derivatives of the fields ϕ and τ, and the viscous dissipation, which is proportional to the laplacian of the fields ϕ and τ. This is a clarifying example that in principle it is necessary to include suitable renormalizations in the parameters of a model when changing the resolution JT, in order to keep correspondence with the resulting dynamics [50]. In our case the values of T_E^H and T_E^{crit} obtained for the adopted resolutions are nevertheless rather similar. In a related framework, see [29] for a detailed discussion of the effects of changing the truncation order for the structure of the bifurcations of a model.

We suspect that plenty of unstable periodic orbits and invariant tori coexist with the attractor of model (A.4)–(A.9) for sufficiently large T_E. Indeed, from the right panel of Fig. 2 we deduce that the Hadley equilibrium undergoes several other bifurcations after the first one. Since the number of unstable eigenvalues of the Hadley equilibrium increases at each Hopf bifurcation, the periodic orbits that branch off have unstable manifolds of increasingly high dimension. Moreover, these unstable periodic orbits in turn undergo Hopf bifurcations, where unstable two-tori branch off, compare [78, Sec. 5]. It seems, therefore, that the phase space quickly gets crowded with high dimensional unstable invariant manifolds.

3.2. Lyapunov exponents and dimension of the strange attractor

To characterize the dynamical properties of the strange attractors of (A.4)–(A.9) we resort to the study of the Lyapunov exponents [20,57], denoted by $\lambda_1 \geq \lambda_2 \geq \cdots \geq \lambda_N$, $N = 6 \times JT$. The maximal exponent λ_1 becomes positive as T_E crosses the torus breakdown value T_E^{crit}, and then increases monotonically with T_E.

The spectrum of the Lyapunov exponents is plotted in the left panel of Fig. 3 for three different values of T_E, again with

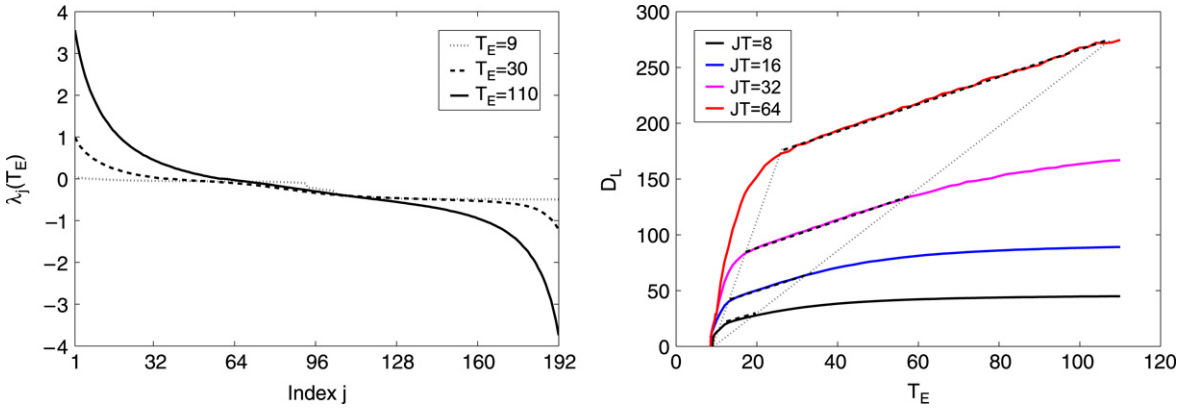

Fig. 3. Left: Spectrum of the Lyapunov exponents for $T_E = 9$, $T_E = 30$, and $T_E = 110$. Units as for λ_j and T_E as described in Table 1. Right: Lyapunov dimension of the attractor of (A.4)–(A.9) as a function of T_E for $JT = 8$, 16, 32, and 64. All the straight lines are parallel and the domain of validity of the linear fit is apparently homothetic.

$JT = 32$. Note that despite the great simplifications adopted in this work, the obtained Lyapunov spectra are qualitatively similar to what reported in [75,80], where a much larger number of degrees of freedom was considered. The distribution of the exponents approaches a smooth shape for large T_E and a similar shape is observed for $JT = 64$ (not shown). This suggests the existence of a well-defined *infinite baroclinicity* model obtained from (6) and (7) as a (possibly, singular perturbation) limit for $T_E \to \infty$. We will analyze elsewhere this mathematical property.

3.2.1. Dimension of the strange attractor

The Lyapunov exponents are used to compute the Lyapunov dimension (also called Kaplan–Yorke dimension, see [20, 41]) and metric entropy (also known as Kolmogorov–Sinai entropy [20]). The Lyapunov dimension is defined by

$$D_L = k + \frac{\sum_{j=1}^{k} \lambda_j}{|\lambda_{k+1}|}, \tag{11}$$

where k is the unique index such that $\sum_{j=1}^{k} \lambda_j \geq 0$ and $\sum_{j=1}^{k+1} \lambda_j < 0$. Under general assumptions on the dynamical system under examination, D_L is an upper bound for the Hausdorff dimension of an attractor.

We have also computed (not shown) other numerical estimates for the dimension of an attractor: the correlation and information dimensions [25]. However, these estimates become completely meaningless when the Lyapunov dimension increases beyond, say, 20, and issues of reliability arise also below 10. In particular, the correlation and information algorithms drastically underestimate the dimension. This is a well-known problem: for large dimensions, prohibitively long time series have to be used. Ruelle [66] suggests as a rule of thumb that a time series of 10^d statistically independent data are need in order to estimate an attractor of dimension d. Therefore, computational time and memory constraints in fact limit the applicability of correlation-like algorithms only to low dimensional attractors.

Both the number of positive Lyapunov exponents and the Lyapunov dimension increase with T_E. As shown in the right panel of Fig. 3, for all the considered values of JT, it is possible to distinguish three regimes of variation of D_L as a function of T_E:

- For small values of $(T_E - T_E^{\text{crit}})$, $D_L \propto (T_E - T_E^{\text{crit}})^{\gamma}$, with γ ranging from $\sim$0.5 ($JT = 8$) to $\sim$0.7 ($JT = 64$). The range of T_E where this behavior can be detected increases with JT.
- For larger values of T_E a linear scaling regime $D_L \sim \beta T_E + \text{const.}$ is found. For all JT, the linear coefficient is remarkably close to $\beta \sim 1.2$. The domain of validity of the linear approximation is apparently homothetic.
- For T_E larger than a JT-dependent threshold, there occurs a sort of phase–space saturation as the Lyapunov dimension begins to increase sublinearly with T_E. Note that while for $JT = 8$ the model is in this regime in most of the explored T_E-domain ($T_E \gtrsim 20$), for $JT = 64$ the threshold is reached only for $T_E \gtrsim 108$. Further discussions on this point will be given in Sections 3.3 and 4.

3.2.2. Metric entropy

The metric entropy $h(\rho)$ of an ergodic invariant measure ρ expresses the mean rate of information creation, see [20] for definition and other properties. If a dynamical system possesses a SRB invariant measure ρ, then Pesin's identity holds:

$$h(\rho) = \sum_{\lambda_j > 0} \lambda_j. \tag{12}$$

However, existence of an SRB measure is rather difficult to demonstrate for a given non-hyperbolic attractor [20,64]. At practical level it is enough to invoke the beneficial role of a small numerical noise [65]; we then refer to the sum of the positive Lyapunov exponents as metric entropy.

The maximal Lyapunov exponent and the metric entropy as functions of T_E are compared for $JT = 8$, 16, 32, and 64 in Fig. 4. It turns out that, for fixed JT, λ_1 increases sublinearly with T_E, whereas the metric entropy has a marked linear dependence $h \sim \beta(T_E - T_E^{\text{crit}})$, with β ranging from $\sim$0.15 ($JT = 8$) to $\sim$0.5 ($JT = 64$). Moreover, for a given value of T_E, the metric entropy increases with JT, whereas for T_E fixed, λ_1 decreases for increasing values of JT. From the dynamical viewpoint, this means on one hand that the maximal sensitivity

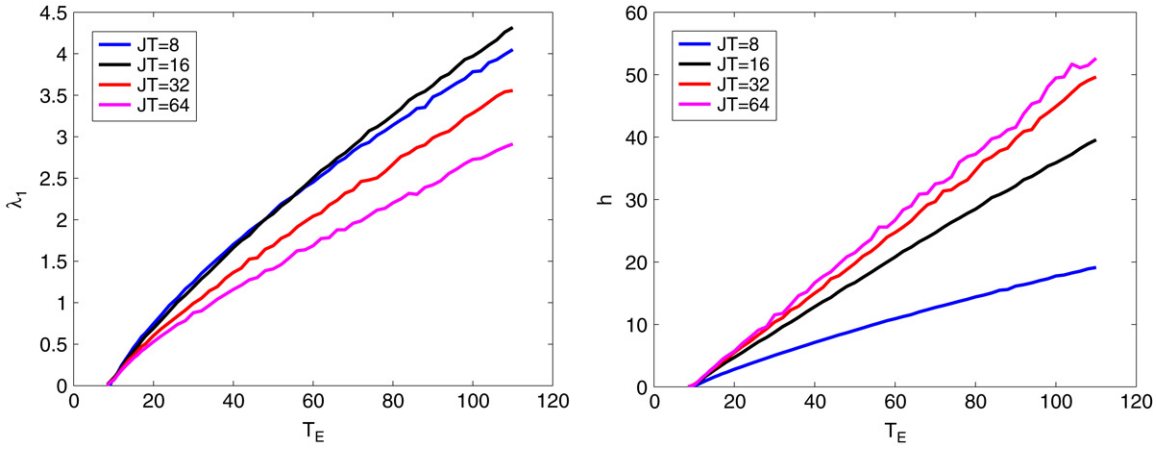

Fig. 4. Left: Maximal Lyapunov exponent on the attractor of (A.4)–(A.9) as a function of T_E for $JT = 8, 16, 32, 64$. Right: Metric entropy. Linear dependences $h \sim \beta(T_E - T_E^{\text{crit}})$ occur for all values of JT.

of the system to variations in the initial condition along a *single direction* is largest for $JT = 8$. On the other hand, there are many more *active degrees of freedom* for $JT = 64$ and they collectively produce a faster *forgetting* of the initial condition as time goes on.

A more precise assessment of the time scales of the system and of predictability fluctuations could be gained by computing generalized Lyapunov exponents and performing the related multifractal diagnostics [4,7,18], which is outside the scope of this paper.

3.3. Bounding box of the attractor

The bounding box of a set of points in an N-dimensional space is defined as the smallest hyperparallelepiped containing the considered set [74]. For clarity, in the N-dimensional phase space, where $N = 6 \times JT$, the volume V_{BB} is computed as:

$$V_{BB} = \prod_{k=1}^{N=6\times JT} \left[\max_{t_{\text{tr}}<t<t_{\max}} (z_k(t)) - \min_{t_{\text{tr}}<t<t_{\max}} (z_k(t)) \right]. \quad (13)$$

Here the z_k denote the $6 \times JT$ variables spanning the phase space of the system, in our case the Fourier coefficients A_j^1, A_j^2, B_j^1, B_j^2, m_j, and U_j, with $j = 1, \ldots, JT$. The condition $t > t_{\text{tr}}$ allows for the transients to die out. Typically, t_{tr} is rather safely fixed to 1500, which correspond to about five years.

When the Hadley equilibrium is the universal attractor, the volume V_{BB} is zero, while it is non-zero if the computed orbit is attracted to a periodic orbit, a two-torus or a strange attractor. We observe that the volume of the bounding box is not an indicator of chaoticity, but only provides a measure of the bulk size of the attractor in phase space. In our case, it turns out that V_{BB} always grows very regularly with T_E. Specifically, each of the factors in the product (13) increases with T_E, so that expansion occurs in all directions of the phase space. This matches the basic expectations on the behavior of a dissipative system having a larger input of energy.

In the right panel of Fig. 5 we present a plot of $\log(V_{BB})$ as function of T_E for the selected values of $JT = 8, 16, 32$, and 64. In the case $JT = 8$, V_{BB} obeys with great precision the power law $V_{BB} \propto (T_E - T_E^{\text{crit}})^{\gamma}$ in the whole domain $T_E \geq 9$. The best estimate for the exponent is $\gamma \sim 40$. Given that the total number of Fourier components is $6 \times JT = 48$, this implies that the growth of the each side of the bounding box is on the average proportional to about the 5/6th power of $(T_E - T_E^{\text{crit}})$.

Table 4
Power-law fits of the volume of the bounding box as $V_{BB} \propto (T_E - T_E^{\text{crit}})^{\gamma}$ in two different ranges of $T_E - T_E^{\text{crit}}$ for each of the considered orders of truncation JT

JT	$\gamma[\log(T_E - T_E^{\text{crit}}) \leq 0.5]$	$\gamma[\log(T_E - T_E^{\text{crit}}) \geq 0.5]$
8	40±1	40±1
16	33±3	80±1
32	66±2	160±1
64	133±4	320±1

See text and Fig. 5 for details.

For higher values of JT, two sharply distinct and well-defined power-law regimes occur. For $JT = 16$, in the lower range of $(T_E - T_E^{\text{crit}})$ – corresponding in all cases to $T_E \lesssim T_E^{\text{crit}} + 1.5$ – the volume of the bounding box increases with about the 35th power of $(T_E - T_E^{\text{crit}})$, while in the upper range of $(T_E - T_E^{\text{crit}})$ – for $T_E \gtrsim T_E^{\text{crit}} + 1.5$ – the power-law exponent abruptly jumps up to about 80. For $JT = 32$ the same regimes can be recognized, but the values of the best estimates of the exponents are twice as large as what obtained with $JT = 16$. Similarly, for $JT = 64$ the best estimates of the exponents are twice as large as for $JT = 32$. The results on the power-law fits of $V_{BB} \propto (T_E - T_E^{\text{crit}})^{\gamma}$ are summarized in Table 4. We emphasize that in all cases the uncertainties on γ, which have been evaluated with a standard bootstrap technique, are rather low and total to less than 3% of the best estimate of γ. Moreover, the uncertainty of the power-law fit greatly worsens if we detune the value of T_E^{crit} by as little as 0.3, thus reinforcing the idea that fitting a power law against the logarithm of $(T_E - T_E^{\text{crit}})$ is a robust choice.

When considering separately the various sides of the bounding box hyperparallelepiped (not shown), *i.e.*, each of the factors in the product (13), we have that for $JT = 8$ all of them increase as about $(T_E - T_E^{\text{crit}})^{5/6}$ in the whole range.

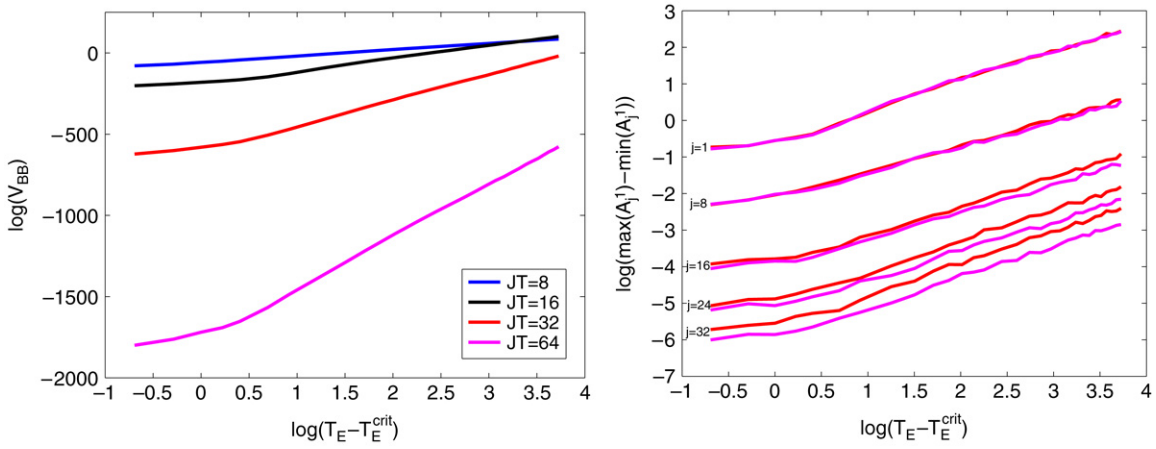

Fig. 5. Left: Volume of the bounding box V_{BB} of the attractor as a function of the detuning parameter $T_E - T_E^{\mathrm{crit}}$ for $JT = 8$, 16, 32, 64. For description of the power-law fits, see the text and Table 4. Right: Value of the corresponding sides of the bounding box pertaining to the variables A_j^1 for $JT = 32$ (red lines) and 64 (magenta lines). Notice the two power-law regimes mentioned in the text. (For interpretation of the references to colour in this figure legend, the reader is referred to the web version of this article.)

For $JT = 16$, 32, and 64, in the lower range of T_E each side of the bounding box increases as about the 1/3rd power of $(T_E - T_E^{\mathrm{crit}})$, while in the upper range of T_E each side of the bounding box increases as about the 5/6th power of $(T_E - T_E^{\mathrm{crit}})$. Selected cases are depicted in the right panel of Fig. 5. So for a given value of truncation order JT, the ratios between the ranges of the various degrees of freedom are essentially unchanged when varying T_E, so that the system obeys a sort of self-similar scaling with T_E.

Summarizing, for sufficiently high truncation order ($JT \geq 16$) a robust parametric dependence is detected for the volume of the bounding box as a function of T_E:

$$V_{BB} \propto (T_E - T_E^{\mathrm{crit}})^{\gamma}, \quad \gamma = \epsilon N$$
$$\epsilon \sim \begin{cases} 1/3, & T_E - T_E^{\mathrm{crit}} \lesssim 1.5, \\ 5/6, & T_E - T_E^{\mathrm{crit}} \gtrsim 1.5, \end{cases} \tag{14}$$

where $N = 6 \times JT$ is the number degrees of freedom.

The comparison, for, say, $JT = 16$ and 32, of factors in (13) having the same order for the same value of $T_E - T_E^{\mathrm{crit}}$ provides insight about the sensitivity to model resolution. In the following discussion, we examine the variables A_j^1 but similar observations apply to all other variables A_j^2, B_j^1, B_j^2, U_j, and m_j. The factors related to the gravest modes, such as $[\max(A_j^1(t)) - \min(A_1^1(t))]$, agree with high precision, thus suggesting that the large scale behavior of the system is only slightly affected by variation of model resolution. When considering the terms related to the fastest latitudinally varying modes allowed by both truncation orders, such as $[\max(A_j^1(t)) - \min(A_j^1(t))]$ with $17 \leq j \leq 32$, we have that those obtained for $JT = 32$ are *larger* than the corresponding factors obtained for $JT = 64$, and the distance between pairs of the same order increases with j. See the right panel of Fig. 5. This is likely to be the effect of spectral saturation: the dynamics contained in the scales which are resolved in the higher resolution models are projected in the fastest modes of the model with lower resolution. The same effect is observed when comparing, for $JT = 16$ and 32, coefficients of the same order such as $[\max(A_j^1(t)) - \min(A_j^1(t))]$ with $9 \leq j \leq 16$. The $JT = 8$ case does not precisely match this picture.

4. Statistical properties of the total energy and zonal wind

In terms of studying the model (A.4)–(A.9), the analysis of the statistics of observables having a direct physical significance is complementary to the investigation performed in Section 3.2, where we have considered properties of special relevance for a dynamical system-oriented analysis. Today, concepts and tools borrowed from dynamical systems theory have widespread applications in the context of modern weather forecast methods, where specific strategies are considered for the local exploration of the phase space of atmospheric models [40]. Since we want to deal with easily readable global physical quantities, we consider the *total energy* and the average *zonal wind* of the model.

4.1. Total energy

The total energy of the system $E(t)$ is a global observable of obvious physical significance, statistically obeying a balance between the external forcing and the internal and surface dissipation. The horizontal energy density of the two-layer QG system can be expressed as follows:

$$\begin{aligned} e(x, y, t) &= \frac{\delta p}{g}\left[\frac{1}{2}\left(\vec{\nabla}\psi_1\right)^2\right. \\ &\quad \left. + \frac{1}{2}\left(\vec{\nabla}\psi_3\right)^2 + \frac{1}{2H_2^2}(\psi_1 - \psi_3)^2\right] \\ &= \frac{\delta p}{g}\left[\left(\vec{\nabla}\phi\right)^2 + \left(\vec{\nabla}\tau\right)^2 + \frac{2}{H_2^2}\tau^2\right]. \end{aligned} \tag{15}$$

Here the factor $\delta p/g$ is the mass per unit surface in each layer, the last term and the first two terms inside the brackets represent

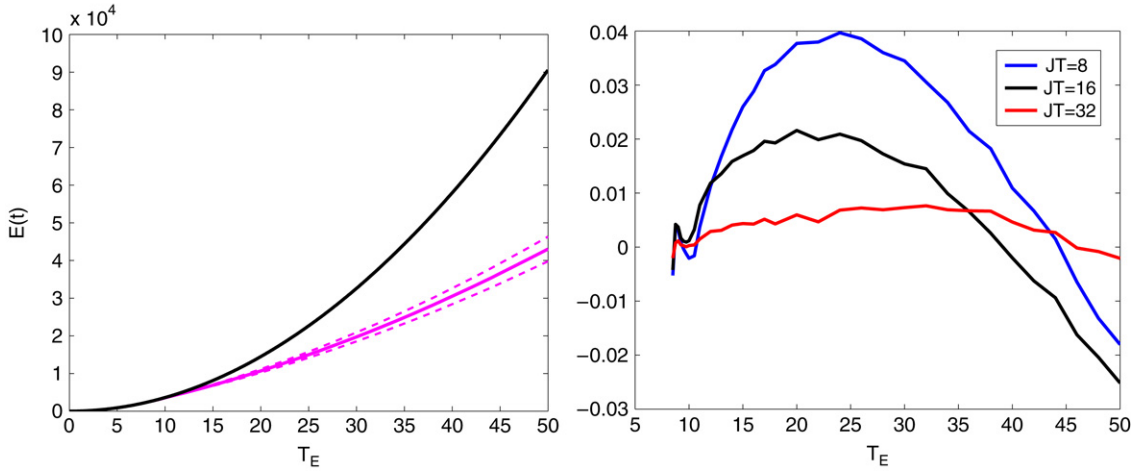

Fig. 6. Left: $\overline{E(t)}$ for the Hadley equilibrium (black line) and deduced from the observed fields in the chaotic regime for $JT = 64$ (magenta line); the magenta dashed line delimit the σ-confidence interval. Right: fractional deviations of $\overline{E(t)}$, for $JT = 8$, 16, and 32, with respect to $JT = 64$. See text for details. (For interpretation of the references to colour in this figure legend, the reader is referred to the web version of this article.)

the potential and kinetic energy, respectively, thus featuring a clear similarity with the functional form of the energy of a harmonic oscillator. Note that in (15) the potential energy term is half of that reported in [58], which contains a trivial algebraic mistake in the derivation of the energy density, as discussed with the author of the book. We then consider as observable the total energy $E(t)$, evaluated by integrating the energy density expression (15):

$$E(t) = \int_0^{L_y}\int_0^{L_x} e(x,y,t)\mathrm{d}x\mathrm{d}y = 6\int_0^{L_y}\int_0^{\frac{2\pi}{\chi}} e(x,y,t)\mathrm{d}x\mathrm{d}y. \quad (16)$$

Potential energy is injected into the system by zonally symmetric baroclinic forcing $\tau^\star$, part of it is transformed into wave kinetic energy by baroclinic conversion, and kinetic energy is eventually dissipated by friction such as that determined by Ekman pumping. This constitutes the Lorenz energy cycle [45,59], which has been analyzed for this system in [78]. In Table 1 we report the conversion factor of the total energy between the non-dimensional and dimensional units.

For the Hadley equilibrium, the time-independent expression for the total energy is:

$$E(t) = E = \frac{\delta p}{g} L_x L_y \left(\frac{RT_E}{4f_0}\frac{1}{1+\frac{\kappa}{\nu_E}\left(\frac{\pi}{L_y}\right)^2}\right)^2 \times \left(\frac{\pi^2}{L_y^2}+\frac{1}{H_2^2}\right). \quad (17)$$

The total energy is proportional to T_E^2 and is mostly (95%) stored as potential energy, which is described by the second term of the sum in (17).

In Fig. 6 we present the results obtained for the various values of JT used in this work. In the left panel we present the $JT = 64$ case, which is representative of that obtained also in the other cases. The time-averaged total energy is monotonically increasing with T_E, but when the system enters the chaotic regime, $\overline{E(t)}$ is much lower than the value for the coexisting Hadley equilibrium. This behavior may be related to the much larger dissipation fuelled by the chaos-driven activation of the smaller scales. In the chaotic regime $E(t)$ is characterized by temporal variability, which becomes more and more pronounced for larger values of T_E.

In the right panel of Fig. 6 we compare the cases $JT = 8$, 16, 32 with respect to $JT = 64$. The overall agreement of $\overline{E(t)}$, where $\overline{X}$ denotes the time average of the field X, is good but progressively worsens when decreasing JT: for $JT = 32$, the maximal fractional difference is less than 0.01, while for $JT = 8$ it is about one order of magnitude larger. Differences among the representations given by the various truncations levels also emerge in power-law fits such as $\overline{E(t)} \propto T_E^\gamma$. In the regime where the Hadley equilibrium is attracting, this fit is exact, with exponent $\gamma = 2$. For $T_E - T_E^{\mathrm{crit}} \lesssim 1.5$ and $T_E > T_E^H$ (the value of the first Hopf bifurcation, see Table 3), for all the values of JT the power-law fit is good, with $\gamma = 1.90 \pm 0.03$, so that a weakly subquadratic growth is realized. For $T_E - T_E^{\mathrm{crit}} \gtrsim 1.5$, only the $JT = 32$ and 64 simulations of $\overline{E(t)}$ obey with excellent approximation a weaker power law, with $\gamma = 1.52 \pm 0.02$ in both cases, while the cases $JT = 8$ and 16 do not satisfactorily fit any power law.

The agreement worsens in the upper range of T_E, which points at the criticality of the truncation level when strong forcings are imposed. Nevertheless, the observed differences are strikingly small between the cases, say, $JT = 8$ and $JT = 64$, with respect to what could be guessed by looking at the Lyapunov dimension, metric entropy, and bounding box volume diagnostics analyzed in the previous sections.

4.2. Zonal wind

Let $U(y,t) = 1/2\,(u_1(y,t) + u_3(y,t))$ be the zonal average of the mean of the zonal wind at the two pressure levels p_1

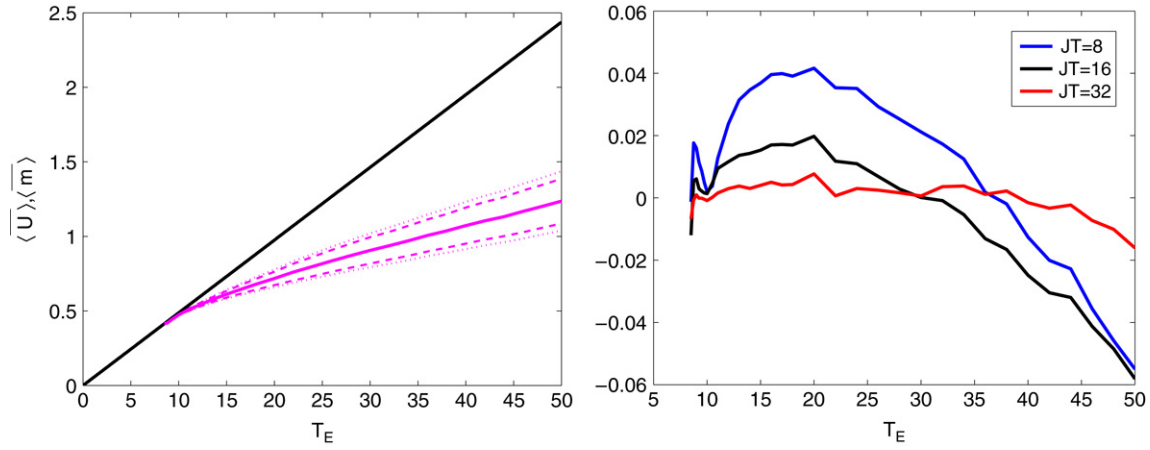

Fig. 7. Left: $\overline{\langle U\rangle} = \overline{\langle m\rangle}$ for the Hadley equilibrium (black line) and deduced from the observed fields in the chaotic regime for $JT = 64$ (magenta line); the magenta dashed and dotted lines delimit the σ-confidence interval for $\langle U\rangle$ and $\langle m\rangle$, respectively. Right: fractional deviations of $\overline{\langle U\rangle} = \overline{\langle m\rangle}$ for $JT = 8$, 16, and 32 with respect to $JT = 64$. See text for details. (For interpretation of the references to colour in this figure legend, the reader is referred to the web version of this article.)

and p_3 and $m(y,t) = 1/2\,(u_1(y,t) - u_3(y,t))$ be the zonal average of the halved difference of the zonal wind at the two pressure levels p_1 and p_3. We here examine the latitudinal average, denoted by $\langle\bullet\rangle$, of U and m:

$$\langle U(y,t)\rangle = \frac{1}{L}\int_0^L U(y,t)\mathrm{d}y = \frac{2}{\pi}\sum_{j=1,\,j\ \mathrm{odd}}^{JT}\frac{U^j}{j}, \tag{18}$$

$$\langle m(y,t)\rangle = \frac{1}{L}\int_0^L m(y,t)\mathrm{d}y = \frac{2}{\pi}\sum_{j=1,\,j\ \mathrm{odd}}^{JT}\frac{m^j}{j}. \tag{19}$$

We have that $\langle U(y,t)\rangle$ is proportional to the total zonal momentum of the atmosphere, whereas $\langle m(y,t)\rangle$, by geostrophy, is proportional to the zonally averaged temperature difference between the northern and the southern boundaries of the domain. Computation of such space averages at the time-independent Hadley equilibrium is straightforward:

$$\langle m(y)\rangle = \langle U(y)\rangle = \frac{R}{f_0 L_y}\frac{T_E}{2}\frac{1}{1+\frac{\kappa}{\nu_N}\left(\frac{\pi}{L_y}\right)^2}. \tag{20}$$

Since we cannot have net, long-term zonal forces acting on the atmosphere at the surface interface, the spatial average of the zonal wind at the pressure level p_3 must be zero. Therefore, the outputs of the numerical integrations must satisfy the constraint $\overline{\langle m(y,t)\rangle} = \overline{\langle U(y,t)\rangle}$, which is automatically satisfied at the Hadley equilibrium. The results of the integration – where such constraint is obeyed within numerical precision – are presented in Fig. 7. In the left panel we plot the outputs for $JT = 64$, which, similarly to the total energy case, is well representative of all the JT cases. The average winds are monotonically increasing with T_E, but, when the system enters the chaotic regimes, the averages $\overline{\langle m(y,t)\rangle} = \overline{\langle U(y,t)\rangle}$ have a much smaller value than at the Hadley equilibrium, and they display sublinear growth with T_E. Moreover, for $T_E > T_E^{\mathrm{crit}}$ the temporal variability of the time series $\langle m(y,t)\rangle$ and $\langle U(y,t)\rangle$ increases with T_E. The variability of $\langle m(y,t)\rangle$ results to be slightly larger than that of $\langle U(y,t)\rangle$, probably because the latter is related to a *bulk* mechanical property of the system such as the total zonal momentum.

The effects of lowering JT are illustrated in Fig. 7 right. The overall agreement, expressed by a small value of the fractional differences, progressively worsens for smaller JT. Notice the similarity of the functional shapes with Fig. 6 right. The results in Fig. 7 right can be summarized as follows: the coarser-resolution models have higher total temperature difference between the two boundaries for values of T_E up to about 30 and lower temperature differences for higher values of T_E. This implies that while for $T_E \lesssim 30$ the latitudinal heat transport increases with JT as a positive trade-off between the higher number of unstable baroclinic modes (within a sloppy linear thinking) or, better, smaller scale baroclinic conversion processes taking place in a higher dimensional attractor, and the enhancement of the barotropic and viscous stabilizing effects, for $T_E \gtrsim 30$ the converse is true.

Again, differences between the various truncations levels emerge as one attempts power-law fits of the form $\overline{\langle m(y,t)\rangle} = \overline{\langle U(y,t)\rangle} \propto T_E^{\gamma}$. For the Hadley equilibrium regime we have $\gamma = 1$. For $T_E \lesssim 10$ and above the first Hopf bifurcation, for all values of JT the power-law fit is good, with $\gamma = 0.875 \pm 0.005$. For $T_E - T_E^{\mathrm{crit}} \gtrsim 1.5$, only the simulations with $JT = 32$ and 64 obey a power law (with $\gamma = 0.58 \pm 0.02$) with excellent approximation, while the realizations of the $JT = 8$ and 16 cases do not fit any power law.

Since we are dealing with a QG system, these observations on the wind fields imply that while the time-averaged meridional temperature difference between the northern and southern boundary of the system increases monotonically with T_E, as to be expected, the realized value is greatly reduced by the onset of the chaotic regime with respect to the corresponding Hadley equilibrium. This is the signature of the negative feedback due to the following mechanism: when the poleward eddy transport of heat is realized, it causes the reduction of the meridional temperature gradient, thus limiting by geostrophy the wind shear, which causes in

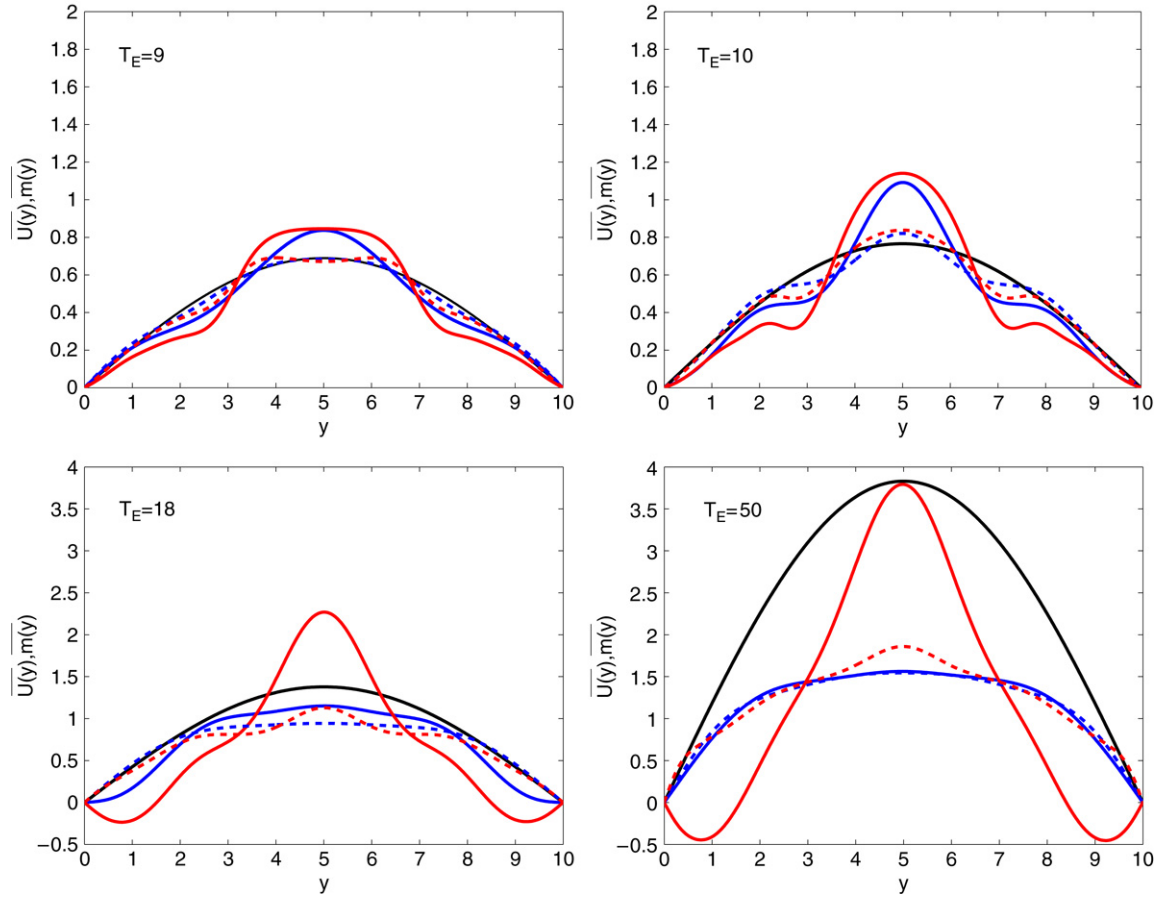

Fig. 8. Time-averaged latitudinal profiles $\overline{U(y)}$ (solid lines) and $\overline{m(y)}$ (dashed lines). In all figures the black solid line indicates the $U(y) = m(y)$ profile of the Hadley equilibrium, the blue and red lines refer to the cases $JT = 8$ and $JT = 32$, respectively. The values of T_E are indicated. Note that the vertical scale for $T_E = 9$ and 10 is about 1/2 as for the other two figures. (For interpretation of the references to colour in this figure legend, the reader is referred to the web version of this article.)

turn a reduction of baroclinically induced eddies *towards* the marginal stability [79]. This process can be considered to be the nonlinear generalization of the *baroclinic adjustment* [79], which implies that the system statistically balances near an average state which corresponds to a fixed point which is neutral with respect to baroclinic instability. This type of adjustment often relies on the (sometimes hidden) idea that a variational principle holds concerning the relationship between the heat & momentum fluxes and the basic state gradient as, for example, in classical convection for which it can be proved that the most unstable mode is the one carrying heat most efficiently across the basic state gradient. In fact, such a variational principle does not hold for ordinary baroclinic instability, as it can be proved that the most rapidly growing baroclinic mode is not the one with the highest heat flux. But in this model, as opposed to the general case, the variational assumption in question is essentially correct, since only one zonal wave is considered, and so the fastest growing unstable wave is also the wave transporting northward the largest amount of heat [76,78]. Nevertheless, the adjustment mechanism does not keep the system *close to marginal stability* since for $T_E > T_E^{\mathrm{crit}}$ both the instantaneous and the time-averaged fields of the system are completely different from those realized at the Hadley equilibrium. Also, this result denies the possibility that the time-mean circulation is maintained by eddies which can be parameterized in terms of the time-mean fields.

By examining more detailed diagnostics on the winds, such as the time-averaged latitudinal profiles of $U(y)$ and of $m(y)$ (Fig. 8), relevant differences are observed between $JT = 8$ and the other three cases. Results are presented for $JT = 8$ and $JT = 32$, the latter being representative also of $JT = 16$ and 64. We first note that already for $T_E = 9$ and 10, such that only a weakly chaotic motion is realized, the $\overline{U(y)}$ and $\overline{m(y)}$ profiles feature in both resolutions relevant qualitative differences with respect to the corresponding Hadley equilibrium profile, although symmetry with respect to the center of the channel is obeyed. The $\overline{U(y)}$ and $\overline{m(y)}$ profiles are different (the constraint $\overline{\langle m(y,t)\rangle} = \overline{\langle U(y,t)\rangle}$ being still satisfied), with $\overline{U(y)} > \overline{m(y)}$ at the center and $\overline{U(y)} < \overline{m(y)}$ at the boundaries of the channel. Nevertheless, like for the Hadley equilibrium, both $\overline{U(y)}$ and $\overline{m(y)}$ are positive and are larger at the center of the channel than at the boundaries. Consequently, at pressure level p_1 there is a westerly flow at the center of the channel and easterly flows at the two boundaries, and that at pressure level p_3 the wind is everywhere westerly and peaks at the center of the channel. Such features are more pronounced

for the $JT = 32$ case, where the mechanism of the convergence of zonal momentum is more accurately represented.

For larger values of T_E, the differences between the two truncation levels become more apparent. For $JT = 8$, the observed $\overline{U(y)}$ and $\overline{m(y)}$ profiles tend to flatten in the center of the channel and to become more similar to each other. Therefore, somewhat similarly to the Hadley equilibrium case, the winds at the pressure level p_1 tend to vanish and all the dynamics is restricted to the pressure level p_3. The $\overline{m(y)}$ profiles for $JT = 32$ are quite similar to those of $JT = 8$, even if they peak and reach higher values in the center of the channel and are somewhat smaller at the boundaries. So when a finer resolution is used, a stronger temperature gradient is realized in the channel center. The $\overline{U(y)}$ profiles obtained for $JT = 32$ are instead very different. They feature a strong, well-defined peak in the channel center and negative values near the boundaries. Therefore, the winds in the upper pressure level are strong westerlies, and peak in the center of the channel, while the winds in the lower pressure level feature a relatively strong westerly jet in the center of the channel and two compensating easterly jets at the boundaries. The fact that for higher resolution the wind profiles are less smooth and have more evident jet-like features is related to the more efficient process of eddy zonal momentum flux convergence [43,72], which *keeps the jet together*, and is related to barotropic stabilization [56]. Examination of the latitudinal profiles in Fig. 8 clarifies our choice to extend the latitudinal domain of the model beyond the geometrically and geographically realistic mid-latitude channel. Due to this, the wind fields in the central portion of the domain (the latter corresponds to mid-latitudes and is of primary interest in this work), are rather different than at the boundary regions.

5. Parametric smoothness and self-scaling of the attractor properties with respect to T_E: Modeling the atmospheric jet

If general enough, the scaling properties discussed in Sections 3 and 4 could be of great help in setting up a theory for the overall statistical properties of the GAC and in guiding – on a heuristic basis – both data analysis and realistic simulations. A leading example for this would be the possibility of estimating the sensitivity of the model output with respect to changes in the parameters. Physical insight into the relevant mechanisms can be obtained by considering the main feedback mechanisms setting the average statistical properties of the system, e.g. when changing the forcing T_E from $T_E = T_E^0 > T_E^{\text{crit}}$ to $T_E = T_E^0 + \Delta T_E$. The change in T_E directly causes an increase in the value of m_1 through Newtonian forcing and indirectly an increase in the value of U_1 through equilibration driven by Ekman pumping. The increase in the value of m_1 enhances the baroclinic conversion and so the values of A_j^1, A_j^2, B_j^1, and B_j^2. The eddy stresses, due to the quadratures of the A and B fields, act as feedback by decreasing the value of the m fields through depletion of baroclinicity and by increasing the value of U fields through barotropic convergence, so that the feedback loop is closed. In the chaotic regime, these feedback mechanisms can be thought as constituting the above mentioned generalized type of statistical baroclinic adjustment process, which reduces the average value of the equator-to-pole temperature difference. This process is not reducible to the stationary balances of the classic theory of GAC, since it takes place when the system lives in a strange attractor and for sure adheres more closely at conceptual level to the equilibration of the atmosphere, given the chaotic nature of the latter. The power laws obtained are the macroscopic realization of the envisioned statistical baroclinic adjustment process, which determines the nature and the statistical properties of the system attractor. Preliminary calculations performed by the authors together with Vannitsem (unpublished results) suggest that the power laws presented here hold in general also on simplified yet global models of the atmospheric circulation, so the obtained scalings laws might be very helpful in establishing a sort of bulk *climate theory* for the atmospheric disturbances. Apart from the diagnostic indicators examined in the previous sections, other statistical properties such as, notably, the distribution of extremes of some field variables of the system display similar properties of smoothness and limited variation, as well as being expressed as power-law scalings of T_E [26]. The smoothness property proves to be of especially great help when dealing with statistical inference in the presence of imposed trends in a non-autonomous version of the dynamical system here considered [27].

The fact that all the considered dynamical indicators (Lyapunov exponents and dimension, volume of the attractor bounding box) and physical quantities (total energy and mean zonal wind) feature a smooth, simple dependence with respect to the forcing parameter T_E and a limited variation is at first striking if one keeps in mind the phenomena typically occurring in systems having low dimensional non-hyperbolic strange attractors. Examples are provided by equations modeling laser systems: parameter regions where chaotic output occurs are very often interspersed with *windows of periodicity*, see *e.g.* [32]. In many such cases, the system properties are discontinuous at the boundaries of the phase-locking intervals, since the attracting orbit vanishes (typically through a saddle-node bifurcation) and a strange attractor appears at once. Other examples of discontinuous dependence on external parameters are contained in the enormous literature on *attractor crises* (see [63] and references therein). Analogous types of bifurcations occur in many systems having low dimensional strange attractors: the list includes Hénon-like families [30,73], climate models (see *e.g.*, [9] and references therein), infinite dimensional systems [24]. Also compare [20] and references therein.

The general, crucial point is here that the effect of a lack of smoothness, or anyway of a very sensitive dependence of model statistical properties on the external parameters, or on details of the model representation, would be detrimental for our ability in setting up a GAC theory, as well as entailing dramatic consequences on our ability to model the atmosphere for practical purposes as well. For the present model (A.4)–(A.9), no window of periodicity or any other *statistical pathology* were detected in the smooth scaling range (say, $T_E > 16$), independently of the truncation order. We have also tried slightly different spectral discretization schemes

and integration methods (such as leapfrog or Runge–Kutta 4), but this feature persisted in all cases. The behavior of the system matches the conjectures stated in [1] for general dissipative systems, basically proposing that in spite of the lack of structural stability, the topological changes induced in the attractor by parameter variations are not catastrophic if the dimension of the system is high enough. The implication of the conjectures is that, as the dimension of a dissipative dynamical system is increased, the number of positive Lyapunov exponents increases monotonically, the Lyapunov exponents tend towards continuous change with respect to parameter variation and the number of observable periodic windows decreases. In substance, it would appear that the modelers paradigm described in the introduction could have some rigorous justification. Persistent chaos and smooth-like dependence of the SRB measure with respect to an external parameter thus appears to be typical of high dimensional systems [2]. One of the first remarks hinting at this general property is in [24].

6. Summary, conclusions and future developments

We have described the construction and the dynamical behavior of an *intermediate complexity* model of the atmospheric system. We take as numerical laboratory for the GAC a quasi-geostrophic (QG) model where the mid-latitude atmosphere is taken as being composed of two layers and the β-plane approximation is considered.

A single zonal wave solution is assumed and by a spectral discretization in the latitudinal direction, the latter equation is reduced to a system of $N = 6 \times JT$ ordinary differential equations, where $JT + 1$ is the number of nodes of the (latitudinally speaking) fastest varying base function. We have considered the cases $JT = 8$, 16, 32, and 64. Although relevant ingredients of geometrical and dynamical nature of the real atmospheric circulation are still missing in this simplified theoretical representation, our model features some fundamental processes determining the general circulation of the Earth atmosphere. In particular, the acting processes are the baroclinic conversion, transforming available potential energy into waves; the nonlinear stabilization of the zonal jet; and the thermal diffusion and Ekman pumping-driven viscous dissipation. It is clear that realism in the representation of the atmosphere is not an issue in this work.

When a larger pool of available energy is provided, the dynamics of the system is richer, since the baroclinic conversion process can transfer larger amounts of energy to the disturbances. Correspondingly, by increasing the parameter T_E, which describes the forced equator-to-pole temperature gradient and parameterizes the baroclinic forcing, the overall behavior of the system is greatly altered. The attractor changes from a fixed point to a strange attractor via a finite number of bifurcations, starting with a Hopf bifurcation at $T_E = T_E^H$ determining the loss of stability of the Hadley equilibrium, and a final two-torus breakdown at $T_E = T_E^{\mathrm{crit}}$. The observed route to chaos is qualitatively the same for $JT = 16$, 32, and 64, and the values T_E^H and T_E^{crit} weakly depend on JT (Table 3), while some differences are observed for $JT = 8$.

The strange attractor is studied by means of the Lyapunov exponents. The Lyapunov spectra obtained for $JT = 32$, 64 resemble what obtained in more complex QG models [75, 80]. A striking feature of this dynamical system is the rather smooth dependence on the parameter T_E of all of its dynamical properties. No windows of periodicity have been detected in the chaotic range and this is quite uncommon especially when comparing with low dimensional chaotic systems, such as the Hénon–Pomeau mapping [37,73] or the Lorenz flow [46]. The metric entropy, representing the total dynamical instability, increases linearly with T_E for $T_E > T_E^{\mathrm{crit}}$ for all examined values of JT, and is larger for larger values of JT. The Lyapunov dimension D_L increases with both T_E and JT. In particular, by increasing T_E, initially the dimension grows with a sublinear power law $D_L \propto (T_E - T_E^{\mathrm{crit}})^{\gamma}$, followed by a linear scaling regime, while for large T_E, D_L *saturates*. The fact that the dimensionality of the attractor increases with the total energy of the system (they are both monotonically increasing with T_E) suggests that the system has a positive temperature, in a statistical mechanical sense. For $JT \geq 16$, each side of the bounding box of the attractor increases as $\propto (T_E - T_E^{\mathrm{crit}})^{1/3}$ for $T_E - T_E^{\mathrm{crit}} \lesssim 1.5$ and as $\propto (T_E - T_E^{\mathrm{crit}})^{5/6}$ for larger values of T_E, while for $JT = 8$ only the latter regime is present. Therefore, the ratios of the ranges of the various degrees of freedom remain essentially unchanged when varying T_E, yielding a self-similar scaling property.

We emphasize that from the point of view of representing the dynamical properties of the atmosphere, bifurcations are often studied with two goals:

- identifying sharp regime transitions;
- obtaining reduced models by projection of the equations on the center manifold corresponding to the bifurcation.

In the present model, no sudden and sharp variations (crises) of the attractor have been detected sufficiently far from T_E^{crit}, *i.e.*, in the range of physically relevant parameter values: here the properties of the attractor vary quite smoothly with the external parameter T_E. Furthermore, the large dimensionality of the chaotic attractor leaves little hope that the dynamics can be reduced by projection on some center manifold. Therefore, it seems very unlikely that the signature of the bifurcations at the transition to chaos, of the kind exploited *e.g.* in the context of physical oceanography in a recent book [23], may be detectable in the fully developed strange attractor and may be useful for computing some of its statistical properties.

Our investigation has focused also on observables of more immediate physical interest. When the system enters the chaotic regime, the average total energy and average zonal winds have lower values than those of the corresponding unstable Hadley equilibrium, because the occupation of the faster varying latitudinal modes fuels Ekman pumping-driven viscous dissipation, which acts preferentially on the small scales. The total energy and the average wind field obey with excellent approximation a subquadratic and sublinear power laws $\propto T_E^{\gamma}$, respectively, and are in *quantitative* agreement for all values

of JT, essentially because these quantities are representative of global balances.

We do not expect to find a global uniform parametrically controlled self-scaling of the system statistical properties when, beyond a certain parameter threshold, new physical processes come into play, *e.g.* in our case allowing for a different and differently efficient way of converting available into kinetic energy. The change in the slope observed in all cases for value of $T_E - T_E^{\mathrm{crit}} \approx 1.5$ may then be interpreted as a changeover from a quasi-linear baroclinic activity to a fully chaotic regime. A possible source of break-up of self-similarity of the statistical properties of the attractor with respect to external parameters is resonant behavior, *i.e.* the preferential occurrence of certain physical processes for a bounded range of values of a given parameter. In the case of atmospheric dynamics, this effect might more relevant than the above mentioned onset of windows of periodicity, although in a range of variability which is different from what explored in this paper, namely the low frequency variability [5,6,68]. In this context, using more realistic atmospheric models comprising bottom orography, a physically interesting experiment to be performed with the purpose of finding the break-up of self-similarity is to parametrically tune and detune the statistical onset of the orographic baroclinic energy conversion [10,16, 68], which is in nature a rather different process from the conventional baroclinic conversion, acting on much larger scales (order of 10 000 km in the real atmosphere).

We summarize the main conclusions regarding the physical properties analyzed in this work as follows:

1. the model displays statistical properties having sufficiently smooth and slow dependence in the parameter space – no crises – as well as *robust* with respect to model representation. The observed persistent chaos and smooth-like dependence of the measure might be related to recently established conjectures, such as the *chaotic hypothesis* proposed by Gallavotti and Cohen [17,33] and the ideas proposed in [1,2]. This leaves hope, in the case such properties are confirmed in more articulated models, for the possibility that well-defined tuning of *realistic* models could allow for a successful representation of the baroclinic wave component of the mid-latitude variability. Other components of atmospheric variability, in particular the low frequency variability, may, instead, be characterized by more critical properties, such as resonance, non-propagating behavior, etc.;
2. all of the statistical properties of the model are not only smooth, but can be expressed as power-law scalings with respect to T_E. Therefore, it is possible to invert the functional relationship for, *e.g.*, the mean zonal wind $\overline{\langle U \rangle}$, and parameterize, at least piecewise, all of the other statistical properties with respect to $\overline{\langle U \rangle}$. In general, the self-similarity could be of great help in setting up a theory for the overall statistical properties of the general circulation of the atmosphere and in guiding – on a heuristic basis – both data analysis and realistic simulations, going beyond the unsatisfactory mean field theories and *brute force* approaches. A leading example for this would be the possibility of estimating the sensitivity of the output of the system with respect to changes in the parameters. The analysis of scaling properties is emerging as new paradigm in the study of geophysical systems [69].
3. Self-similarity might result from *statistical equilibration* of the baroclinic conversion process, which provides a modern, statistical version of classical theories of the baroclinic jet. The observed equilibration somewhat resembles the deterministic *baroclinic adjustment* envisaged in the '70s, but takes place through more complex processes occurring in the strange attractor. Given the almost-linear nature of the *wave-zonal flow* interaction, it is possible to establish a simple closure of the properties of propagation and instability of the waves with respect to a *parameterized* zonal wind, which acts as integrator providing a time-varying *index of refraction*.

Three are the main, necessary directions of future work along the proposed line of approach to GAC:

1. Consolidating and explaining the knowledge (see [70]) that in the real atmosphere the dynamics of traveling baroclinic disturbances is dominated by the *wave-zonal flow* interaction and the role of the *wave–wave* interaction is minor. Exploiting the potential of such a finding in modeling in detail the so called *extratropical storm tracks* [38] (see http://data.giss.nasa.gov/stormtracks/ for a nice tutorial), which are the everyday atmospheric manifestation of the baroclinic dynamics we are debating.
2. Along the previous line, analyzing mathematically for this model the action of the zonal wind as an integrator of the wave disturbances. This can be accomplished by writing the approximate evolution equations for the wave fields, indicated generically as $\vec{x}$, in the form $\dot{\vec{x}} = M(t)\vec{x}$, where M is a stochastic matrix [18] written in terms of the U and m fields. The statistical properties of M may inform us on the physical processes responsible for the wave dynamics. The generation and decay processes are quite relevant for the mid-latitudes of the real atmosphere, because we have 2D wavenumber–frequency spectral densities that only vaguely correspond, in a statistical sense, to well-defined dispersion relations $\omega = \omega(k)$, since at all frequencies the spectral width is relatively wide [21,22,53].
3. Analyzing all the debated properties in more articulated numerical models. Some preliminary results in this sense have been found by the authors and Vannitsem (unpublished results). An important technical issue in this context may be the separation of the properties of the baroclinic mid-latitude jet system from the low frequency variability.

Acknowledgments

The authors wish to thank M. Felici, G. Gallavotti, V. Gupta, S. Lovejoy, P. Malguzzi, L. Smith, A. Tsonis, and S. Vannitsem for scientific hints and encouragement, and the two reviewers for relevant suggestions aimed at the improvement of the paper. V.L. wishes to thank ISAC-CNR for kind hospitality and the

Centro di Cultura Scientifica A. Volta (Como, Italy) for partial financial support.

Appendix. Evolution equations of the single zonal wave two-layer model and numerical methods

As explained in Section 2, for the purposes of this study we retain the zonally symmetric component plus only one wave component in the zonal direction of the fields $\phi(x, y, t)$ and $\tau(x, y, t)$. Since we intend to represent schematically the baroclinic conversion processes, which in the real atmosphere take place on scales of the order of $L_x/6$ [21,22], we select the wave component having wave vector $\chi = 6 \times 2\pi/L_x$. We then have:

$$\phi(x, y, t) = -\int_{\pi/2}^{y} U(z, t)\mathrm{d}z + A \exp(\mathrm{i}\chi x) + \text{c.c.}, \tag{A.1}$$

$$\tau(x, y, t) = -\int_{\pi/2}^{y} m(z, t)\mathrm{d}z + B \exp(\mathrm{i}\chi x) + \text{c.c.}. \tag{A.2}$$

By substituting (A.1) and (A.2) into equations (6) and (7) and projecting onto the zonal Fourier modes of order $n = 0$ and $n = 6$, we obtain a set of partial differential equations for the 6 real fields A^1, A^2, B^1, B^2, U, m, where A^1 and A^2 are the real and imaginary parts of A, and similarly for B. Vanishing boundary conditions are chosen at $y = 0$, L_y for all fields. In the case of U and m this amounts to setting no-flux boundary conditions for the zonally symmetric component of ϕ and τ, along the lines of Phillips [60]. A Fourier half-sine expansion of the fields is then carried out along y, with time-varying coefficients:

$$X = \sum_{j=1}^{JT} X_j \sin\left(\frac{\pi j y}{L_y}\right), \tag{A.3}$$

where X represents each of the fields A^1, A^2, B^1, B^2, U, and m, and for the truncation order JT we have used the values $JT = 8$, 16, 32, 64. With this definition, and because of (A.1) and (A.2), the latitudinal average of τ and ϕ vanishes in all cases, so that the energy density (15) does not depend on the latitudinal average of τ, which has no physical relevance. By using the expansion (A.3) and projecting on the basis functions $\sin(\frac{\pi j y}{L_y})$, we then obtain a set of $6 \times JT$ ordinary differential equations for A_j^1, A_j^2, B_j^1, B_j^2, U_j, m_j. Particular care must be taken for the nonlinear (quadratic) terms appearing in (6) and (7). Such terms result into sums of quadratic products of the time-dependent variables $A_j^{1/2}$, $B_j^{1/2}$, U_j, m_j times y-dependent factors given by quadratic products of the basis functions $\sin(\frac{\pi j y}{L_y})$ and their derivatives. We define a pseudospectral operator $\Pi_j(\cdot)$ for projecting such quadratic y-dependent terms onto the j-th basis function $\sin\frac{\pi j y}{L_y}$ through Fourier collocation: the factors are evaluated pointwise at the JT equally spaced collocation points $y_1, \ldots, y_{JT}$ in the y-domain. Then, an inverse Discrete Sine Transform is carried out, yielding the Fourier coefficients of the nonlinear terms, thus obtaining the projection. The software library `fftw3`, publicly available at www.fftw.org, has been adopted. The resulting system of ordinary differential equations, which constitutes the base model of our study, is:

$$\begin{aligned}
\dot{A}_j^1 = \frac{1}{\chi^2 + w_j^2}\Bigg[& -\frac{2\nu_E}{H_2^2}(\chi^2 + w_j^2)A_j^1 - \chi\beta A_j^2 \\
& + \frac{2\nu_E}{H_2^2}(\chi^2 + w_j^2)B_j^1 + \Pi_j\Big(-\chi U A_{yy}^2 + \chi^3 U A^2 \\
& + \chi U_{yy} A^2 - \chi m B_{yy}^2 + \chi^3 m B^2 + \chi m_{yy} B^2\Big)\Bigg],
\end{aligned} \tag{A.4}$$

$$\begin{aligned}
\dot{A}_j^2 = \frac{1}{\chi^2 + w_j^2}\Bigg[& -\frac{2\nu_E}{H_2^2}(\chi^2 + w_j^2)A_j^2 + \chi\beta A_j^1 \\
& + \frac{2\nu_E}{H_2^2}(\chi^2 + w_j^2)B_j^2 + \Pi_j\Big(\chi U A_{yy}^1 - \chi^3 U A^1 \\
& - \chi U_{yy} A^1 + \chi m B_{yy}^1 - \chi^3 m B^1 - \chi m_{yy} B^1\Big)\Bigg],
\end{aligned} \tag{A.5}$$

$$\begin{aligned}
\dot{B}_j^1 = \frac{1}{\chi^2 + w_j^2 + \frac{2}{H_2^2}}\Bigg[& -\left(\frac{2\nu_E}{H_2^2} + \frac{2\kappa}{H_2^2}\right)(\chi^2 + w_j^2)B_j^1 \\
& - \chi\beta B_j^2 + \frac{2\nu_E}{H_2^2}(\chi^2 + w_j^2)A_j^1 + \Pi_j\Bigg(- \chi U B_{yy}^2 \\
& + \chi^3 U B^2 + \chi U_{yy} B^2 + \frac{2}{H_2^2}\chi U B^2 - \chi m A_{yy}^2 \\
& + \chi^3 m A^2 + \chi m_{yy} A^2 - \frac{2}{H_2^2}\chi m A^2\Bigg)\Bigg],
\end{aligned} \tag{A.6}$$

$$\begin{aligned}
\dot{B}_j^2 = \frac{1}{\chi^2 + w_j^2 + \frac{2}{H_2^2}}\Bigg[& -\left(\frac{2\nu_E}{H_2^2} + \frac{2\kappa}{H_2^2}\right)(\chi^2 + w_j^2)B_j^2 \\
& + \chi\beta B_j^1 + \frac{2\nu_E}{H_2^2}(\chi^2 + w_j^2)A_j^2 + \Pi_j\Bigg(\chi U B_{yy}^1 \\
& - \chi^3 U B^1 - \chi U_{yy} B^1 - \frac{2}{H_2^2}\chi U B^1 + \chi m A_{yy}^1 \\
& - \chi^3 m A^1 - \chi m_{yy} A^1 + \frac{2}{H_2^2}\chi m A^1\Bigg)\Bigg],
\end{aligned} \tag{A.7}$$

$$\begin{aligned}
\dot{U}_j = & -\frac{2\nu_E}{H_2^2}(U_j - m_j) - 2\chi\Pi_j \\
& \times\left(-A^1 A_{yy}^2 + A^2 A_{yy}^1 - B^1 B_{yy}^2 + B^2 B_{yy}^1\right),
\end{aligned} \tag{A.8}$$

$$\begin{aligned}
\dot{m}_j = \frac{1}{\frac{2}{H_2^2} + w_j^2}\Bigg[& -w_j^2\frac{2\kappa}{H_2^2}m_j + w_j^2\frac{2\nu_E}{H_2^2}(U_j - m_j) \\
& - \frac{2\nu_N}{H_2^2}(m_j - m_j^*) + \Pi_j\Bigg(4\chi\frac{1}{H_2^2}(A^1 B^2 - A^2 B^1)_{yy} \\
& + 2\chi(-A^1 B_{yy}^2 + A^2 B_{yy}^1 - B^1 A_{yy}^2 \\
& - B^2 A_{yy}^1)_{yy}\Bigg)\Bigg],
\end{aligned} \tag{A.9}$$

where the explicit expression of the projected nonlinear terms is not presented here because of space limitation. The numerical solution of the system (A.4)–(A.9) is computed

with a standard Runge–Kutta–Fehlberg(4,5) algorithm [71] with adaptive step size, where the approximated solution is carried by the order five method. The local truncation error is kept below $1 \cdot e - 6$. The step size adjustment procedure is similar to that of DOPRI5, available at (www.unige.ch/~hairer).

For the computation of the averages $\overline{X}$, time series of 315 360 adimensional time units (1000 years in natural units) have been computed for all values of JT, after discarding a transient of 5 years. The observables $E(t)$, $U(y,t)$, and $m(y,t)$ have been sampled every 0.216 time units (four times a day), thereby obtaining time series of 1 460 000 elements.

References

[1] D.J. Albers, J.C. Sprott, Structural stability and hyperbolicity violation in high-dimensional dynamical systems, Nonlinearity 19 (2006) 1801–1847.

[2] D.J. Albers, J.C. Sprott, J.P. Crutchfield, Persistent chaos in high dimensions, Phys. Rev. E 74 (2006) 057201.

[3] T.L. Bell, Climate sensitivity from fluctuation dissipation: Some simple model tests, J. Atmospheric Sci. 37 (1980) 1700–1707.

[4] R. Benzi, G. Paladin, G. Parisi, A. Vulpiani, Characterisation of intermittency in chaotic systems, J. Phys. A 18 (1985) 2157–2165.

[5] R. Benzi, P. Malguzzi, A. Speranza, A. Sutera, The statistical properties of general atmospheric circulation: Observational evidence and a minimal theory of bimodality, Q. J. R. Meteorol. Soc. 112 (1986) 661–674.

[6] R. Benzi, A. Speranza, Statistical properties of low frequency variability in the Northern Hemisphere, J. Clim. 2 (1989) 367–379.

[7] G. Boffetta, P. Giuliani, G. Paladin, A. Vulpiani, An extension of the Lyapunov analysis for the predictability problem, J. Atmospheric Sci. 55 (1998) 3495–3507.

[8] G. Boffetta, G. Lacorata, S. Musacchio, A. Vulpiani, Relaxation of finite perturbations: Beyond the fluctuation–response relation, Chaos 13 (2003) 806–812.

[9] H.W. Broer, C. Simó, R. Vitolo, Bifurcations and strange attractors in the Lorenz-84 climate model with seasonal forcing, Nonlinearity 15 (2002) 1205–1267.

[10] A. Buzzi, A. Trevisan, A. Speranza, Instabilities of a baroclinic flow related to topographic forcing, J. Atmospheric Sci. 41 (1984) 637–650.

[11] B. Cessac, J.-A. Sepulchre, Linear response, susceptibility and resonances in chaotic toy models, Physica D 225 (2007) 13–28.

[12] J.G. Charney, The dynamics of long waves in a baroclinic westerly current, J. Atmospheric Sci. 4 (1947) 136–162.

[13] J.G. Charney, On the scale of atmospheric motions, Geofys. Publik. 17 (1948) 251–265.

[14] J.G. Charney, R. Fjörtoft, J. von Neumann, Numerical integration of the barotropic vorticity equation, Tellus 2 (1950) 237–254.

[15] J.G. Charney, J.C. Devore, Multiple flow equilibria in the atmosphere and blocking, J. Atmospheric Sci. 36 (1979) 1205–1216.

[16] J.G. Charney, D.M. Straus, Form-drag instability, multiple equilibria and propagating planetary waves in the baroclinic, orographically forced, planetary wave system, J. Atmospheric Sci. 37 (1980) 1157–1176.

[17] E.G.D. Cohen, G. Gallavotti, Note on two theorems in nonequilibrium statistical mechanics, J. Stat. Phys. 96 (1999) 1343–1349.

[18] A. Crisanti, G. Paladin, A. Vulpiani, Products of Random Matrices in Statistical Physics, Springer, New York, 1993.

[19] E.T. Eady, Long waves and cyclone waves, Tellus 1 (1949) 33–52.

[20] J.-P. Eckmann, D. Ruelle, Ergodic theory of chaos and strange attractors, Rev. Modern Phys. 57 (1985) 617–655.

[21] A. Dell'Aquila, V. Lucarini, P.M. Ruti, S. Calmanti, Hayashi spectra of the northern hemisphere mid-latitude atmospheric variability in the NCEP-NCAR and ECMWF reanalyses, Clim. Dyn. (2005), doi:10.1007/s00382-005-0048-x.

[22] A. Dell'Aquila, P.M. Ruti, S. Calmanti, V. Lucarini, Southern hemisphere mid-latitude atmospheric variability of the NCEP-NCAR and ECMWF reanalyses, J. Geophys. Res. 112 (2007) D08106, doi:10.1029/2006JD007376.

[23] H.A. Dijkstra, Nonlinear Physical Oceanography, Springer, New York, 2005.

[24] J.D. Farmer, Chaotic attractors of an infinite-dimensional dynamic system, Physica D 4 (1982) 366–393.

[25] J.D. Farmer, E. Ott, J.A. Yorke, The dimension of chaotic attractors, Physica D 7 (1983) 153–180.

[26] M. Felici, V. Lucarini, A. Speranza, R. Vitolo, Extreme value statistics of the total energy in an intermediate complexity model of the mid-latitude atmospheric Jet. Part I: Stationary case, J. Atmos. Sci. 64 (2007) 2137–2158, doi:10.1175/JAS3895.1.

[27] M. Felici, V. Lucarini, A. Speranza, R. Vitolo, Extreme value statistics of the total energy in an intermediate complexity model of the mid-latitude atmospheric Jet. Part I: Trend detection and assessment, J. Atmos. Sci. 64 (2007) 2159–2175, doi:10.1175/JAS4043.1.

[28] C. Foias, E.J. Olson, Finite fractal dimension and Holder–Lipschitz parametrization, Indiana Univ. Math. J. 45 (1996) 603–616.

[29] V. Franceschini, C. Tebaldi, Truncations to 12, 14 and 18 modes of the Navier–Stokes equations on a two-dimensional torus, Meccanica 20 (1985) 207–230.

[30] J.M. Freitas, F. Alves, M.P. Carvalho, Statistical stability for Henon maps of the Benedicks–Carleson type, (2006). Preprint arXivmath.DS/0610602.

[31] P.K. Friz, J.C. Robinson, Parametrising the attractor of the two-dimensional Navier–Stokes equations with a finite number of nodal values, Physica D 148 (2001) 201–220.

[32] C. Bonatto, J.C. Garreau, J.A.C. Gallas, Self-similarities in the frequency–amplitude space of a loss-modulated CO_2 laser, Phys. Rev. Lett. 95 (2005) 143905.

[33] G. Gallavotti, Chaotic hypothesis: Onsager reciprocity and fluctuation–dissipation theorem, J. Stat. Phys. 84 (1996) 899–926.

[34] M. Ghil, R. Benzi, G. Parisi (Eds.), Turbulence and Predictability in Geophysical Fluid Dynamics and Climate Dynamics, North-Holland, Amsterdam, 1985.

[35] I.M. Held, The gap between simulation and understanding in climate modeling, Bull. Am. Meteorol. Soc. (2005) 1609–1614.

[36] I.M. Held, A.Y. Hou, Nonlinear axially symmetric circulations in a nearly inviscid atmosphere, J. Atmospheric Sci. 37 (1980) 515–533.

[37] M. Hénon, Y. Pomeau, Two strange attractors with a simple structure, in: Turbulence and Navier–Stokes Equations, vol. 565, Springer-Verlag, 1976, pp. 29–68.

[38] B.J. Hoskins, P.J. Valdes, On the existence of storm-tracks, J. Atmospheric Sci. 47 (1990) 1854–1864.

[39] Intergovernmental Panel on Climate Change 2001, Working Group I, Climate Change 2001: The Scientific Basis, Cambridge University Press, Cambridge, 2001.

[40] E. Kalnay, Atmospheric Modeling, Data Assimilation and Predictability, Cambridge Univ. Press, Cambridge, 2003.

[41] J. Kaplan, J. Yorke, Chaotic behaviour of multidimensional difference equations, in: Functional Differential Equations and Approximations of Fixed Points, Springer LNM, 1979, pp. 204–227.

[42] R. Kubo, The fluctuation dissipation theorem, Rep. Progr. Phys. 29 (1966) 255–284.

[43] H.L. Kuo, Dynamics of quasigeostrophic flows and instability theory, Adv. Appl. Mech. 13 (1973) 247–330.

[44] C.E. Leith, Climate response and fluctuation dissipation, J. Atmospheric Sci. 32 (1975) 2022–2026.

[45] E.N. Lorenz, Available potential energy and the maintenance of the general circulation, Tellus 7 (1955) 157–167.

[46] E.N. Lorenz, Deterministic nonperiodic flow, J. Atmospheric Sci. 20 (1963) 130–141.

[47] E.N. Lorenz, The Nature and Theory of the General Circulation of the Atmosphere, World Meteorol. Organ., Geneva, 1967.

[48] E.N. Lorenz, The predictability of a flow which possesses many scales of motion, Tellus 21 (1969) 289–307.

[49] E.N. Lorenz, Forced and free variations of weather and climate, J. Atmospheric Sci. 36 (1979) 1367–1376.
[50] E.N. Lorenz, Attractor sets and quasi-geostrophic equilibrium, J. Atmospheric Sci. 37 (1980) 1685–1699.
[51] V. Lucarini, Towards a definition of climate science, Int. J. Environ. Pollut. 18 (2002) 409–414.
[52] V. Lucarini, J.J. Saarinen, K.-E. Peiponen, E. Vartiainen, Kramers–Kronig Relations in Optical Materials Research, Springer, Heidelberg, 2005.
[53] V. Lucarini, S. Calmanti, A. Dell'Aquila, P.M. Ruti, A. Speranza, Intercomparison of the northern hemisphere winter mid-latitude atmospheric variability of the IPCC models, Clim. Dyn. 28 (2007) 829–848, doi:10.1007/s00382-006-0213-x.
[54] P. Malguzzi, A. Trevisan, A. Speranza, Statistics and predictability for an intermediate dimensionality model of the baroclinic jet, Ann. Geophys. 8 (1990) 29–35.
[55] R. Mantovani, A. Speranza, Baroclinic instability of a symmetric, rotating, stratified flow: A study of the nonlinear stabilisation mechanisms in the presence of viscosity, Nonlinear Proc. Geophys. 9 (2002) 487–496.
[56] N. Nakamura, Momentum flux, flow symmetry, and the nonlinear barotropic governor, J. Atmospheric Sci. 50 (1993) 2159–2179.
[57] V.I. Oseledec, A multiplicative ergodic theorem. Lyapunov characteristic numbers for dynamical systems, Trudy Mosk. Mat. Obs. (Moscow Math. Soc.) 19 (1968) 19.
[58] J. Pedlosky, Geophysical Fluid Dynamics, 2nd ed., Springer-Verlag, New York, 1987.
[59] J.P. Peixoto, A.H. Oort, Physics of Climate, Am. Inst. of Phys., College Park, 1992.
[60] N.A. Phillips, Energy transformations and meridional circulations associated with simple baroclinic waves in a two-level, quasi-geostrophic model, Tellus 6 (1954) 273–286.
[61] A. Randriamampianina, W.-G. Früh, P. Maubert, P.L. Read, DNS of bifurcations to low-dimensional chaos in an air-filled rotating baroclinic annulus (2005). Preprint at http://www-atm.physics.ox.ac.uk/user/read/.
[62] C.H. Reick, Linear response of the Lorenz system, Phys. Rev. E 66 (2002) 036103.
[63] C. Robert, K.T. Alligood, E. Ott, J.A. Yorke, Explosions of chaotic sets, Physica D: Nonlinear Phenom. 144 (1–2) (2000) 44–61.
[64] D. Ruelle, What are the measures describing turbulence? Progr. Theoret. Phys. Suppl. 64 (1978) 339–345.
[65] D. Ruelle, Chaotic Evolution and Strange Attractors, Cambridge University Press, Cambridge, 1989.
[66] D. Ruelle, Deterministic chaos: The science and the fiction, Proc. R. Soc. Lond. A 427 (1990) 241–248.
[67] D. Ruelle, General linear response formula in statistical mechanics, and the fluctuation–dissipation theorem far from equilibrium, Phys. Lett. A 245 (1998) 220–224.
[68] P.M. Ruti, V. Lucarini, A. Dell'Aquila, S. Calmanti, A. Speranza, Does the subtropical jet catalyze the mid-latitude atmospheric regimes? Geophys. Res. Lett. 33 (2006) L06814.
[69] D. Schertzer, S. Lovejoy, Uncertainty and predictability in geophysics: Chaos and multifractal insights, in: The State of the Planet: Frontiers and Challenges in Geophysics, American Geophysical Union, Washington, 2004.
[70] T. Schneider, The general circulation of the atmosphere, Ann. Rev. Earth Plan. Sci. 34 (2006) 655–688, doi:10.1146/annurev.earth.34.031405.125144.
[71] L.F. Shampine, H.A. Watts, S. Davenport, Solving non-stiff ordinary differential equations — The state of the art, SIAM Rev. 18 (1976) 376–411.
[72] A.J. Simmons, B.J. Hoskins, The life cycles of some nonlinear baroclinic waves, J. Atmospheric Sci. 35 (1978) 414–432.
[73] C. Simó, On the Hénon–Pomeau attractor, J. Stat. Phys. 21 (1979) 465–494.
[74] L.A. Smith, Disentangling uncertainty and error: On the predictability of nonlinear systems, in: A. Mees (Ed.), Nonlinear Dynamics and Statistics, Birkhauser, Boston, 2000, pp. 31–64.
[75] C. Snyder, T.M. Hamill, Leading Lyapunov vectors of a turbulent baroclinic jet in a quasigeostrophic model, J. Atmospheric Sci. 60 (2003) 683–688.
[76] A. Speranza, Deterministic and statistical properties of the westerlies, Paleogeophysics 121 (1983) 511–562.
[77] A. Speranza, V. Lucarini, Environmental science: Physical principles and applications, in: F. Bassani, J. Liedl, P. Wyder (Eds.), Encyclopedia of Condensed Matter Physics, Elsevier, Amsterdam, The Netherlands, ISBN: 0-12-227610-8, 2005.
[78] A. Speranza, P. Malguzzi, The statistical properties of a zonal jet in a baroclinic atmosphere: A semilinear approach. Part I: Two-layer model atmosphere, J. Atmospheric Sci. 48 (1988) 3046–3061.
[79] P.H. Stone, Baroclinic adjustment, J. Atmospheric Sci. 35 (1978) 561–571.
[80] S. Vannitsem, C. Nicolis, Lyapunov vectors and error growth patterns in a T21L3 quasigeostrophic model, J. Atmospheric Sci. 54 (1997) 347–361.
[81] L.S. Young, What are SRB measures, and which dynamical systems have them? J. Stat. Phys. 108 (5) (2002) 733–754.